1299 Eugene A. Bendgman

NATIONAL ADVISORY COMMITTEE FOR AERONAUTICS

TECHNICAL NOTE

No. 1299

EFFECTS OF MACH NUMBER AND REYNOLDS NUMBER ON THE MAXIMUM LIFT COEFFICIENT OF A WING OF NACA 230-SERIES AIRFOIL SECTIONS

By G. Chester Furlong and James E. Fitzpatrick

Langley Memorial Aeronautical Laboratory
Langley Field, Va.

LIBRARY COPY
2 1 1993
LANGLEY RESEARCH CENTER
LIBRARY NASA
HAMPTON, VIRGINIA

Washington
May 1947

FOR REFERENCE
NOT TO BE TAKEN FROM THIS ROOM

3 1176 01425 8173

NATIONAL ADVISORY COMMITTEE FOR AERONAUTICS

TECHNICAL NOTE NO. 1299

EFFECTS OF MACH NUMBER AND REYNOLDS NUMBER ON THE MAXIMUM LIFT COEFFICIENT OF A WING OF NACA 230-SERIES AIRFOIL SECTIONS

By G. Chester Furlong and James E. Fitzpatrick

SUMMARY

The effects of Mach number and Reynolds number on the maximum lift coefficient of a wing of NACA 230-series airfoil sections are presented. The ranges of Mach number for the wind-tunnel tests were from 0.10 to 0.35 and from 0.08 to 0.27; the corresponding Reynolds number ranges were from 1,530,000 to 4,530,000 and from 2,450,000 to 7,880,000, respectively.

The wing was tested with full-span and partial-span split flaps deflected 60° and without flaps. Leading-edge-roughness tests were made with the flaps-retracted configuration. Some chordwise pressure-distribution measurements were made for all flap configurations of the model.

The results of the tests indicated that peak values of maximum lift coefficient were obtained at relatively low free-stream Mach numbers (approx. 0.20 for the flaps-deflected configurations and 0.25 to 0.30 for the flaps-retracted configuration) and occurred when the critical pressure coefficient was reached on the upper surface of the wing. The values of maximum lift coefficient were increased by increasing Reynolds number or deflecting the flaps, but in both cases the critical pressure coefficient was reached at lower free-stream Mach numbers. After the critical Mach number had been reached, the value of maximum lift coefficient was appreciably reduced and there was an indication that beyond the critical Mach number the effect of Reynolds number on the maximum lift becomes markedly reduced. The value of maximum lift coefficient before the critical Mach number was reached was almost entirely dependent on Reynolds number, but even in the low Mach number range, Mach number effects should not be neglected. Any method, therefore, that is utilized to predict flight values of maximum lift coefficient from wind-tunnel data by accounting for a difference in Reynolds number and neglecting any change in Mach number may give erroneous results.

INTRODUCTION

Estimates of flight values of maximum lift coefficient from wind-tunnel tests are usually made by accounting for the incremental change in lift coefficient that results from differences in Reynolds number. The effects of a variation of Reynolds number on the maximum lift coefficient and the stall phenomenon are described in references 1 and 2. References 3 and 4 indicate that compressibility effects on the maximum lift coefficient may occur at relatively low free-stream Mach numbers (0.20) A knowledge of the interrelated effects of Mach number and Reynolds number on maximum lift coefficient is important in the interpretation of wind-tunnel test data, in flight problems concerning airplane maneuvering performance, and in propeller performance at high thrust conditions. Because of the importance of Mach number as shown in references 3 and 4, any estimated flight values of maximum lift coefficient may be questionable if only the difference in Reynolds number is taken into account. As data concerning these phenomena are incomplete, the present tests have been made to explain further the effects of Mach number and Reynolds number on the maximum lift coefficient of a wing.

The present paper contains the results of tests made with a wing of NACA 230-series airfoil sections in the Langley 19-foot pressure tunnel. The tests were conducted at tunnel pressures of 14.7 and 33 pounds per square inch absolute These tunnel pressures gave Mach number ranges of 0.10 to 0 35 and 0.08 to 0.27. The corresponding Reynolds number ranges were from 1,530,000 to 4,530,000 and from 2,450,000 to 7,880,000, respectively. The tests included force tests and chordwise pressure-distribution measurements at six spanwise stations.

The tests were made with the wing model equipped with full-span and partial-span split flaps deflected 60° and without flaps. In addition, force tests were made with leading-edge roughness for the flaps-retracted configuration.

There are included herein data from tests of this wing in the Langley 16-foot high-speed tunnel, part of which data has been published in reference 5.

SYMBOLS

A	aspect ratio (b^2/S)
C	cross-sectional area of test section, square feet

C_L	lift coefficient (L/q_oS)
$C_{L_{max}}$	maximum lift coefficient
D	diameter of tunnel test section, feet
L	lift, pounds
M_o	free-stream Mach number (V_o/a)
M_{cr}	critical Mach number; free-stream Mach number when local Mach number is 1.00
P	pressure coefficient $\left(\frac{p - p_o}{q_o}\right)$
P_{cr}	critical pressure coefficient; pressure coefficient at a local Mach number of 1.00
R_o	free-stream Reynolds number $\left(\frac{\rho V_o \bar{c}}{\mu}\right)$
S	wing area, square feet
V_o	free-stream velocity, feet per second
a	speed of sound, feet per second
a_c	slope of lift curve in compressible flow $\left(\left(\frac{dC_L}{d\alpha}\right)_c\right)$
a_i	slope of lift curve in incompressible flow $\left(\left(\frac{dC_L}{d\alpha}\right)_i \text{ or } a_c\left(\frac{\beta + \frac{a_o}{\pi A}}{1 + \frac{a_o}{\pi A}}\right) \text{ (see reference 6)}\right)$
a_o	two-dimensional lift-curve slope $\left(dc_l/d\alpha_o\right)$
b	wing span, feet
$\bar{c}$	mean aerodynamic chord (M.A.C.), feet $\left(\frac{2}{S}\int_0^{b/2} c^2\, dy\right)$
c	local chord, feet

c_t	chord of tip section
c_l	section lift coefficient
p	local static pressure, pounds per square foot
p_o	free-stream static pressure, pounds per square foot
$p_{19'}$	pressure in Langley 19-foot pressure tunnel, pounds per square inch absolute
q_o	free-stream dynamic pressure, pounds per square foot
x	distance along local chord from leading edge, feet
y	lateral distance perpendicular to root chord, feet
α	angle of attack (wing root chord), degrees
α_o	section angle of attack, degrees
α_{max}	angle of attack at maximum lift coefficient, degrees
β	compressibility factor $\left(\sqrt{1 - M_o^2}\right)$
δ_f	flap deflection, degrees
δ_w	jet-boundary correction factor (reference 7)
ρ	mass density of air, slugs per cubic foot
μ	coefficient of viscosity of air, pound-seconds per square foot

MODEL, APPARATUS, AND TESTS

Model and Apparatus

A three-view drawing of the wing is presented as figure 1. All pertinent geometric characteristics have been incorporated in this figure. The root section of the wing is an NACA 23016 airfoil section and the construction tip is an NACA 23009 airfoil section. The wing has a span of 12 feet, an aspect ratio of 6, a taper ratio of 2, an aerodynamic washout of 4° (4° geometric washout), a dihedral angle of 0°, and sweepback of 3.2° (one-quarter chord line).

Inasmuch as the wing was of rigid steel construction, no appreciable amounts of deflection or twist were encountered during the tests.

The split flaps tested had a chord 20 percent of the local wing chord. The spans of the full-span and partial-span flaps were 99 percent and 55 percent of the wing span, respectively. Both flaps were deflected 60° with the lower surface of the wing, and the flaps were held in place by blocks. Figure 1 shows the layout of the flaps

The leading-edge roughness was obtained by spraying fine-grained carborundum (No. 60) on freshly applied shellac. The roughness extended across the complete span over a surface length of 8 percent chord measured along the wing surface from the leading edge on both the upper and lower surfaces.

The model was mounted on the normal wing-support system of the Langley 19-foot pressure tunnel. (See fig. 2.) The tips of these supports, or that part extending up from the support fairings, were designed to duplicate those used in the tests of reference 5. The aerodynamic forces and moments were measured by a simultaneous-recording six-component balance system.

The wing contained 33 surface-pressure orifices at each of the six spanwise stations. Figure 1 shows the spanwise location of the stations and a typical chordwise distribution of pressure orifices. The pressure leads were conducted internally to a pipe protruding from the root-chord trailing edge (fig. 1). From the trailing edge, the pressure leads were taken to multiple-tube manometers through a specially designed tube-transfer system. This system, which is shown in figure 3, allowed continuous testing through the angle-of-attack range without necessitating manual adjustments. The tube-transfer system, however, did not allow force tests to be made simultaneously with pressure measurements and, consequently, force tests were made with the system removed. During the force tests a short fairing cap covered the pipe extending from the root-chord trailing edge.

Tests

Tests were conducted at two tunnel pressures of 14.7 and 33 pounds per square inch absolute. The ranges of Mach number and Reynolds number thus obtained are

Tunnel pressure (lb/sq in.)	Mach number range	Reynolds number range
14.7	0.10 to 0.35	1,530,000 to 4,530,000
33	0.08 to 0.27	2,450,000 to 7,880,000

For convenience, tests made at tunnel pressures of 14.7 and 33 pounds per square inch absolute are designated $p_{19'} = 14.7$ and $p_{19'} = 33$, respectively.

Tare tests were made for all model flap configurations at both tunnel pressures. In addition, scale effect on tares was investigated for the flaps-retracted configuration. The results indicated no change in tare through the Mach number and Reynolds number ranges obtainable in the Langley 19-foot pressure tunnel.

Force tests were made through the tunnel-speed range at both tunnel pressures for all flap configurations. Leading-edge-roughness tests were also made at both tunnel pressures for the flaps-retracted configuration. The force tests at a tunnel pressure of 33 pounds per square inch absolute were made at speeds which would produce either the same Mach numbers or Reynolds numbers as those of similar tests reported in reference 5.

A comparison of the maximum-lift-coefficient data obtained in the two wind tunnels for the same test conditions was made. A Langley 16-foot high-speed tunnel condition (Mach number of 0.15 and Reynolds number of 2,450,000) was reproduced in the Langley 19-foot pressure tunnel at a tunnel pressure of 16.5 pounds per square inch absolute.

Chordwise-pressure-distribution measurements were made at $p_{19'} = 33$ for values of Mach number and Reynolds number obtained in force tests.

Visual observations of the stall pattern were made by tuft surveys at several tunnel airspeeds.

The wing was tested through an angle-of-attack range from -3.7° through the stall. A constant value of Mach number or Reynolds number was maintained during a run by proper adjustment of the dynamic pressure to account for changes in temperature and pressure.

CORRECTIONS TO DATA

Force Tests

The lift coefficients have been corrected for support-strut interference as determined by tare tests.

The angles of attack have been corrected for air-stream misalinement and jet-boundary effects. The air-stream misalinement was determined during the tare tests, and the jet-boundary correction was determined by the following equation derived from reference 8:

$$\Delta\alpha = \left(1 + \frac{1.05c}{D\beta}\right) \delta_w \frac{S}{C} 57.3C_L$$

This equation contains the angle-of-attack correction at the lifting line for the case of a wing with an elliptical spanwise load distribution and also an additional correction for the induced streamline curvature. The term β has been introduced to account for compressibility effects (reference 6). For the tests in the Langley 19-foot pressure tunnel, a mean value of β was found to suffice and the correction to angle of attack becomes $0.6780C_L$.

Pressure Distribution

No corrections have been applied to the local values of static pressure. The local effects of the struts and walls on these pressures are assumed to be negligible. In the computation of the pressure coefficients, however, average dynamic pressure and free-stream static pressure across the span have been used.

RESULTS

The variation of Mach number with Reynolds number obtained from tests reported in reference 5 of the same wing as tested herein and obtained at both tunnel pressures in the Langley 19-foot pressure tunnel is shown in figure 4. All values of Reynolds number have been based on the mean aerodynamic chord of the wing. The maximum deviations of Mach number and Reynolds number from the curves for these tests in the Langley 19-foot pressure tunnel are within values of $M_o = \pm 0.01$ and $R_o = \pm 20{,}000$.

The lift-coefficient data obtained from force tests in the Langley 19-foot pressure tunnel are presented in figure 5. This figure includes data for four configurations, that is, for flaps retracted, for partial-span flaps, for full-span flaps, and for flaps retracted with leading-edge roughness at both the Langley 19-foot pressure tunnel conditions.

A check run to determine the values of maximum lift coefficient

that would be obtained in the two tunnels under the same test conditions gave a value of maximum lift coefficient of 1.35, as compared with a value of 1.36 (reference 5) obtained in the Langley 16-foot high-speed tunnel. This agreement was considered satisfactory and justified any conclusions interpreted from the results of both tunnels.

The slopes of the lift curves for the flaps-retracted configuration with and without leading-edge roughness and the slopes corrected to incompressible-flow conditions by the method of reference 6 are plotted against Reynolds number in figure 6. The figure shows the applicability of the correction factor of reference 6 in converting slopes of these lift curves from compressible-flow conditions to incompressible-flow conditions. After the correction factor had been applied to the slopes, the results from the Langley 16-foot high-speed tunnel (reference 5) and the Langley 19-foot pressure tunnel were in excellent agreement.

The maximum lift coefficients and corresponding angles of attack have been plotted against Mach number and Reynolds number in figure 7, which also includes data obtained from reference 5. The variations of maximum lift coefficient with Mach number and Reynolds number for all model configurations and tunnel conditions resemble those shown in reference 4 for a wing of NACA 0012 airfoil section. Figure 7 shows that for each tunnel condition the maximum lift coefficient increases with an increase in airspeed - R and M increasing (see fig. 4) - to a maximum or peak value, after which the maximum lift coefficient decreases with a further increase in airspeed. The peak values of maximum lift coefficient occur at Mach numbers of approximately 0.20 for the flaps-deflected configurations and between 0.25 and 0.30 for the flaps-retracted configuration. There were no peak maximum lift coefficients for the flaps-retracted leading-edge-roughness configuration in the Mach number ranges obtainable in the Langley 19-foot pressure tunnel. A comparison of the flaps-deflected configurations (figs. 7(b) and 7(c)) with the flaps-retracted configuration (fig. 7(a)) at similar tunnel conditions shows that flap deflection causes the peak maximum lift coefficients to occur at lower Mach numbers. For each model configuration a similar comparison between the two tunnel conditions $p_{19'} = 33$ and $p_{19'} = 14.7$ shows that the peak maximum lift coefficients occur at lower Mach numbers for $p_{19'} = 33$ than for $p_{19'} = 14.7$.

Some of the chordwise pressure-distribution data obtained during the tests are presented for three of the six spanwise stations in figures 8 to 12. Pressure-distribution data were

obtained in the Langley 19-foot pressure tunnel for only the tunnel condition $p_{19'} = 33$ as some atmospheric-pressure data were available from tests in the Langley 16-foot high-speed tunnel. The data are presented at the maximum angles of attack for several values of Mach number and Reynolds number with flaps retracted and deflected. A comparison was made of data from the Langley 16-foot high-speed tunnel with data from the Langley 19-foot pressure tunnel ($p_{19'} = 33$) at comparable values of either Mach number or Reynolds number. As a result of the large pressure peaks encountered with flaps deflected, the pressure-coefficient scale has been reduced from that used for the flaps-retracted configuration.

From the pressure-distribution data that were available from tests of the wing in both tunnels, figure 13 has been prepared. The peak pressure coefficients obtained for each section at the maximum lift coefficient of the wing were first plotted against the semispan to obtain the faired maximum value of peak pressure coefficient on the wing; the maximum peak pressure coefficients of the wing were then plotted against Mach number to obtain figure 13. The figure is not so complete as would be desirable because of the limited Mach number range of the Langley 19-foot pressure tunnel.

The results of the visual stall studies are summarized in figure 14 in which the stall progressions for the flaps-retracted and flaps-deflected configurations are presented.

DISCUSSION

The significance of a variation of Reynolds number alone on the maximum lift coefficient of an airfoil has been fully described in reference 1 in which data are presented of tests conducted at low free-stream Mach numbers ($M_o \approx 0.08$). To reiterate, the effect of increasing Reynolds number is to cause an earlier transition from laminar to turbulent boundary layer. The increased turbulent boundary layer is then capable of resisting separation, and a higher angle of attack is reached before stalling occurs; thus, an increase in maximum lift coefficient is obtained. As pointed out in reference 2, the Reynolds number first affects the lift of an airfoil at moderately high angles of attack. When the Reynolds number has reached a value at which the entire boundary layer has become turbulent, there is evidence that a further increase in Reynolds number will not produce any increase in the maximum lift coefficient.

In the region of the critical Mach number M_{cr} a pronounced change exists in the flow, but whether an actual separation of flow occurs seems to depend on both the type of airfoil involved and the angle of attack at which the critical Mach number is reached.

When, as in the tests of the wing, a variation in Mach number is accompanied by a variation in Reynolds number, the explanation for the variation of $C_{L_{max}}$ is not readily apparent. The most significant point of the variation of $C_{L_{max}}$ with Mach number and Reynolds number is the peak value attained; hence, the determining factor or factors of this point will be discussed first. The peak values of $C_{L_{max}}$ may be determined by the critical Mach number, by the Reynolds number at which the entire boundary layer is turbulent, or by both.

The maximum pressure peaks encountered in tests of the wing have been plotted against Mach number in figure 13. The curve of P_{cr} against Mach number is also shown. The intersections of the curves of maximum pressure coefficient with the curve of P_{cr} occur at free-stream Mach numbers at which the peak values of $C_{L_{max}}$ were obtained in force tests (fig. 7). The probability is indicated that the peak values of $C_{L_{max}}$ for each tunnel condition occurred when the critical Mach number had been reached. The possibility that the Reynolds number at which the entire boundary layer is turbulent would be reached in these tests is excluded. The effect of increasing the magnitude of Reynolds number for a given Mach number, however, by changing from the Langley 16-foot high-speed tunnel condition (reference 5) to the Langley 19-foot pressure tunnel condition of $p_{19'} = 33$ (see fig. 4) increased the peak pressure coefficients - and, consequently, $C_{L_{max}}$ - but reduced slightly the free-stream Mach number (fig. 13) at which the peak value of $C_{L_{max}}$ occurred. When the flaps are deflected, an increase in pressure coefficient along the chord results and this increase causes an increased maximum lift coefficient; but because of the increased pressure peaks, the critical pressure coefficient is reached at lower free-stream Mach numbers with flaps deflected than with flaps retracted.

The foregoing discussion of figure 13 is based on consideration of the maximum pressure coefficient that occurred on the wing.

Visual observations of the stall pattern (fig. 14) justified the discussion of the stall with reference to only one point on the wing. The stall studies were made at several Mach numbers and revealed an abrupt simultaneous stall over the entire surface of the wing.

The decrease in $C_{L_{max}}$ after the peak value has been reached is due to the fact that the critical pressure coefficient diminishes (fig. 13) as the airspeed is increased beyond this point. As the airspeed is increased, therefore, the critical pressure coefficient is reached on the wing at progressively lower angles of attack; early stall is thus precipitated and, consequently, lower values of maximum lift coefficient are obtained. The principal contribution of Reynolds number toward increasing $C_{L_{max}}$, as previously pointed out, is its effect in increasing the angle of attack at which the wing stalls; hence, when the critical Mach number limits the peak value of $C_{L_{max}}$, the effect of a further increase in Reynolds number is markedly reduced. The data from the present tests (figs. 7(a) to 7(c)) are too limited to determine whether at very high airspeeds $C_{L_{max}}$ is affected at all by Reynolds number. Flight tests of an airplane equipped with a wing of NACA 66-series airfoil sections (reference 9) have shown that at values of Mach number in excess of 0.50 the effects of Reynolds number are negligible. The value of Mach number at which the Reynolds number will become negligible will probably depend on the particular airfoil involved.

The increase in $C_{L_{max}}$ before the critical Mach number is reached is due almost entirely to the change in Reynolds number; that is, the natural transition from laminar to turbulent boundary layer with increasing Reynolds number allows higher angles of attack to be reached before the wing stalls. When the values of $C_{L_{max}}$ are compared at equal Reynolds numbers (figs. 7(a) to 7(c)), it is seen that, in the range below the peak value of $C_{L_{max}}$, lower values of $C_{L_{max}}$ are obtained at a tunnel pressure of 14.7 pounds per square inch absolute than are obtained at a tunnel pressure of 33 pounds per square inch absolute. The values at $p_{19'} = 14.7$ are actually at higher Mach numbers than are the values at $p_{19'} = 33$ (fig. 4).

A plausible explanation of this loss in lift due to the increase

in Mach number may be that although the leading-edge pressures at lift coefficients below the stall are almost the same, the transition from laminar to turbulent boundary layer is delayed by the increased Mach number and, since the wing tested exhibited laminar separation, the wing will stall at slightly lower angles of attack. This rearward movement of transition, because of an increase in Mach number, has been determined for the low-drag range at the Ames Laboratory, and a continuation of the discussion to $C_{L_{max}}$ appears reasonable from the results obtained in the present tests.

Reference 1 presents a method for predicting incremental changes in the maximum lift coefficient that occur as a result of the difference between wind-tunnel and flight Reynolds number. Because the flight value of Mach number will usually be somewhat higher than that used as a basis for the method of reference 1 ($M_o \approx 0.08$), the application of that method for the prediction of flight values of $C_{L_{max}}$ from tests at low Reynolds number will probably yield a higher value of $C_{L_{max}}$ - even if the critical Mach number has not been reached.

The preceding discussion has dealt with the effects of Mach number and Reynolds number on the maximum lift coefficient of a wing which has an abrupt stall precipitated by high peak values of leading-edge pressure. The characteristics of a wing with lower peak values of leading-edge pressure and a more complex stall may be materially different. If a wing exhibits a stall produced by trailing-edge separation, the leading-edge pressures may be low enough to allow a rather high free-stream Mach number to be reached before the critical pressure coefficient is encountered. In such a case, the Reynolds number at which a completely turbulent boundary layer exists may be reached before the critical Mach number is attained. The flaps-retracted leading-edge-roughness configuration (fig. 7(d)) is an example in which the complete boundary layer is turbulent. There is very little change in $C_{L_{max}}$ through the Reynolds number range. The peak leading-edge pressures furthermore have probably been reduced so that no critical Mach number is indicated in the range of the present tests. The value of $C_{L_{max}}$ at the lowest Mach number and Reynolds number for $p_{19'} = 14.7$ causes the curve in figure 7(d) to have a sharp drop in the low Reynolds number range. The shape of the lift curve for this test condition (fig. 5(g)) at $C_{L_{max}}$ is such as to suggest the

possibility of premature stall although no cause is evident. Because the drop in the curve of $C_{L_{max}}$ against Reynolds number occurs through a large part of the complete Reynolds number range and is a result of this one test point, the curves have been shown dashed between this test condition and the next highest test condition.

CONCLUDING REMARKS

On the basis of the wind-tunnel investigation made to determine the effects of Mach number and Reynolds number on the maximum lift coefficient of a wing of NACA 230-series airfoil sections, the following conclusions may be drawn. These conclusions appear applicable to other wings which exhibit an abrupt stall precipitated by high leading-edge pressures.

1. The peak values of maximum lift coefficient are determined by a critical Mach number which is attained at relatively low free-stream Mach numbers (approx. 0.20 for the flaps-deflected configurations and 0.25 to 0.30 for the flaps-retracted configuration).

2. The values of maximum lift coefficient are increased when the Reynolds number is increased but the critical pressure coefficient (critical Mach number) is reached at lower free-stream Mach numbers.

3. The increased pressure peaks that result when the flaps are deflected cause the critical pressure coefficient (critical Mach number) to be reached at lower free-stream Mach numbers than when the flaps are retracted.

4. After the critical pressure coefficient (critical Mach number) has been reached, the value of maximum lift coefficient is appreciably reduced by further increase in Mach number and there is an indication that the effect of Reynolds number on the maximum lift becomes markedly reduced.

5. The value of maximum lift coefficient before the critical pressure coefficient (critical Mach number) is reached is almost entirely dependent on Reynolds number, but even in the low Mach number range, Mach number effects should not be neglected. Any method, therefore, that is utilized to predict flight values of maximum lift coefficient from wind-tunnel data by accounting for a difference in Reynolds number and neglecting a difference in Mach number may give erroneous results.

Langley Memorial Aeronautical Laboratory
National Advisory Committee for Aeronautics
Langley Field, Va., November 19, 1946

REFERENCES

1. Jacobs, Eastman N., and Sherman, Albert: Airfoil Section Characteristics as Affected by Variations of the Reynolds Number. NACA Rep. No. 586, 1937.

2. Pinkerton, Robert M.: The Variation with Reynolds Number of Pressure Distribution over an Airfoil Section. NACA Rep. No. 613, 1938.

3. Stack, John, Fedziuk, Henry A., and Cleary, Harold E.: Preliminary Investigation of the Effect of Compressibility on the Maximum Lift Coefficient. NACA ACR, Feb. 1943.

4. Muse, Thomas C.: Some Effects of Reynolds and Mach Numbers on the Lift of an NACA 0012 Rectangular Wing in the NACA 19-Foot Pressure Tunnel. NACA CB No. 3E29, 1943.

5. Pearson, E.O., Jr., Evans, A. J., and West, F. E., Jr.: Effects of Compressibility on the Maximum Lift Characteristics and Spanwise Load Distribution of a 12-Foot-Span Fighter-Type Wing of NACA 230-Series Airfoil Sections. NACA ACR No. L5G10, 1945.

6. Goldstein, S., and Young, A.D.: The Linear Perturbation Theory of Compressible Flow with Applications to Wind-Tunnel Interference. R.& M. No. 1909, British A.R.C., 1943.

7. Silverstein, Abe, and White, James A.: Wind-Tunnel Interference with Particular Reference to Off-Center Positions of the Wing and to the Downwash at the Tail. NACA Rep. No. 547, 1935.

8. Lotz, Irmgard : Correction of Downwash in Wind Tunnels of Circular and Elliptic Sections. NACA TM No. 801, 1936.

9. Spreiter, John R., and Steffen, Paul J.: Effect of Mach and Reynolds Numbers on Maximum Lift Coefficient. NACA TN No. 1044, 1946.

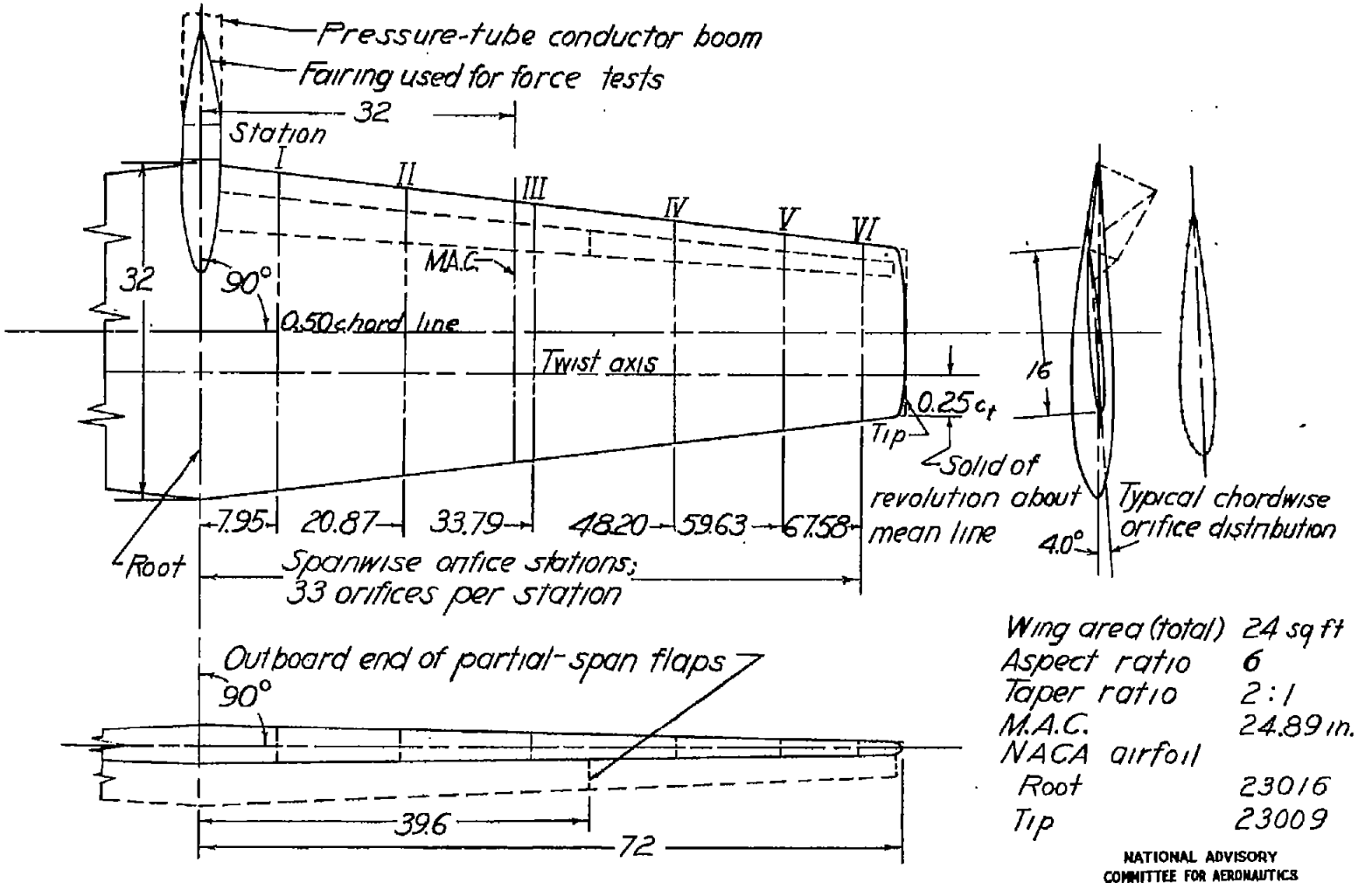

Figure 1.- Layout of wing of NACA 230-series airfoil sections tested in the Langley 19-foot pressure tunnel. Pressure orifices in left wing panel only. (All dimensions are in inches.)

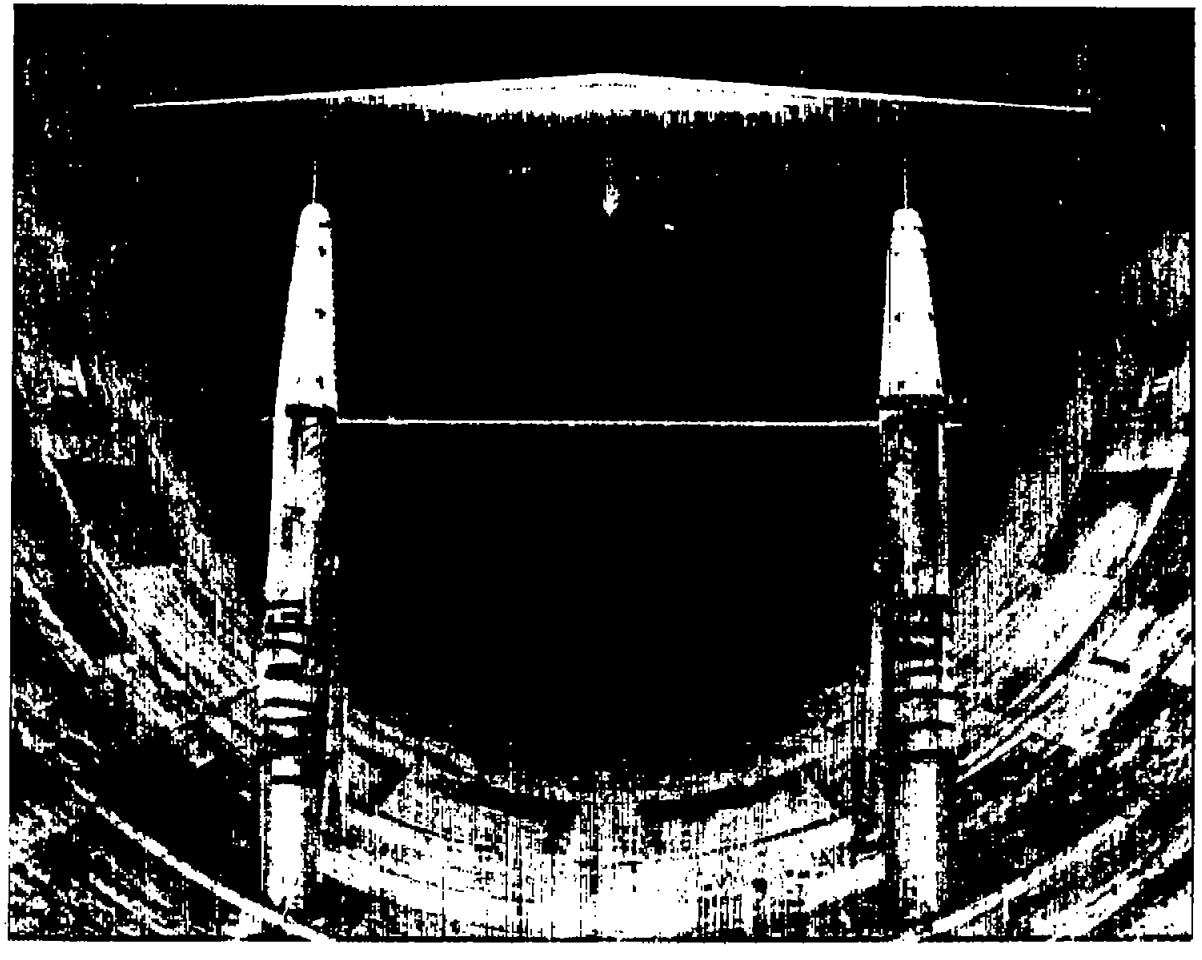

(a) Front view.

Figure 2.- Wing of NACA 230-series airfoil sections mounted in the Langley 19-foot pressure tunnel.

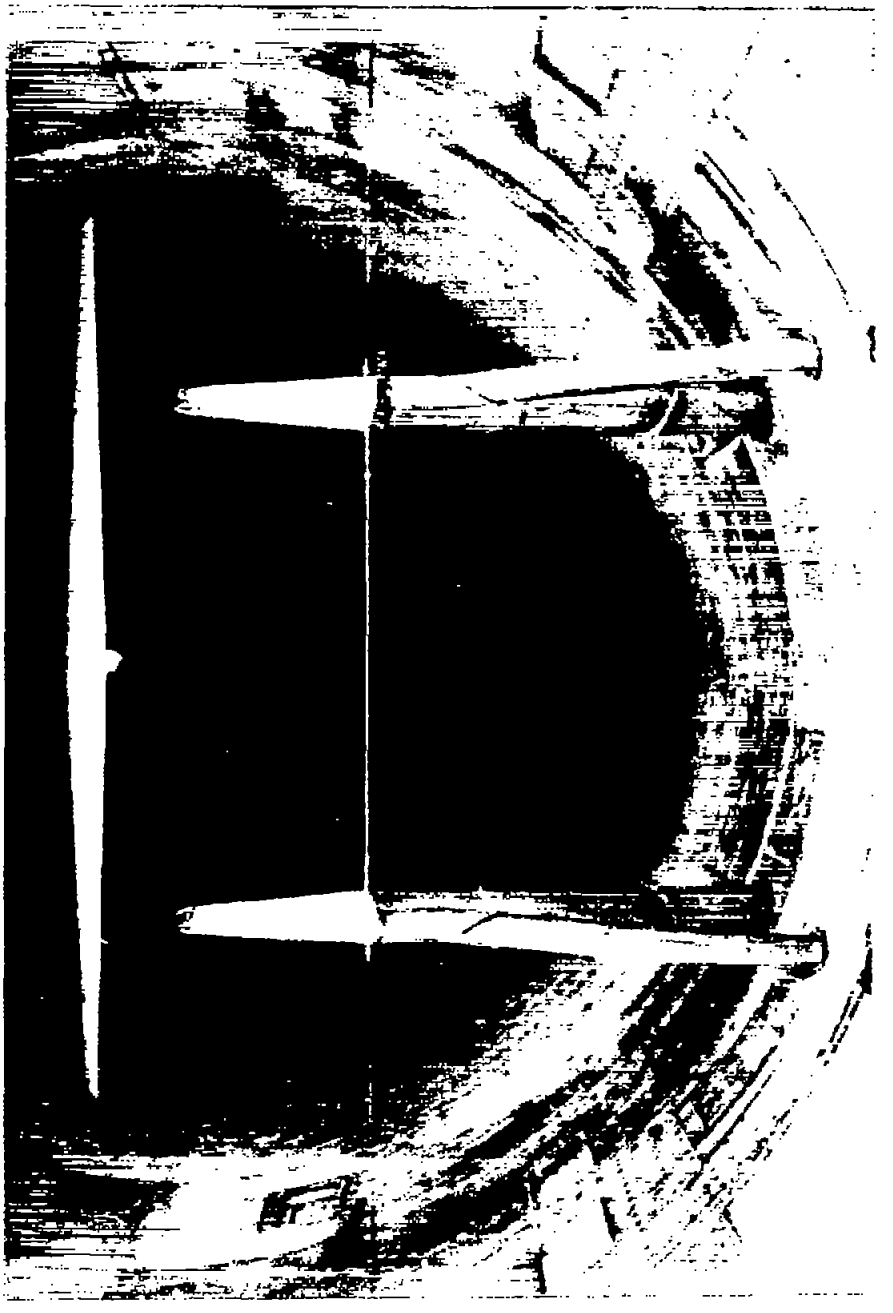

(b) Rear view.

Figure 2.- Concluded.

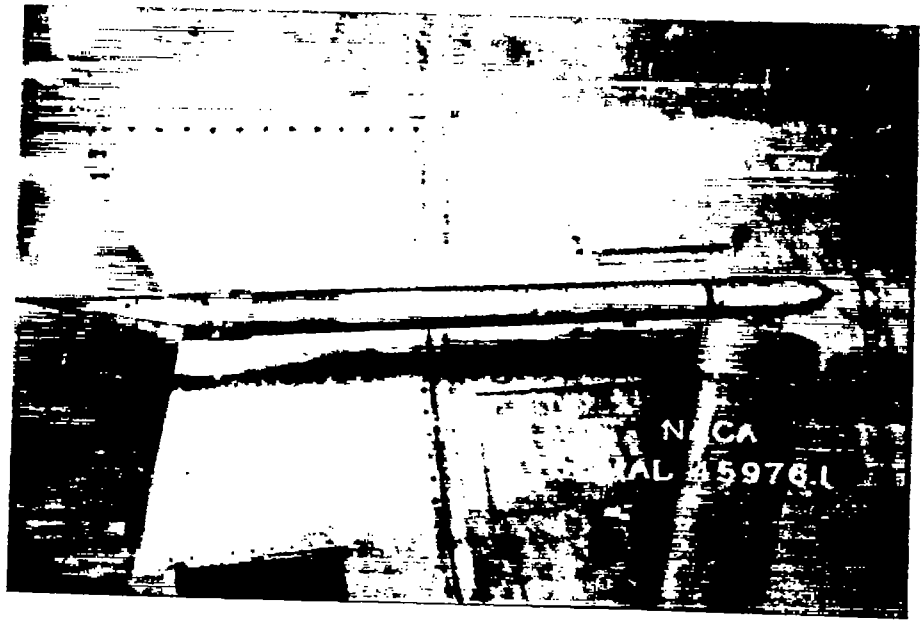

Figure 3.- Close-up of tube-transfer system used in tests of a wing of NACA 230-series airfoil sections in the Langley 19-foot pressure tunnel.

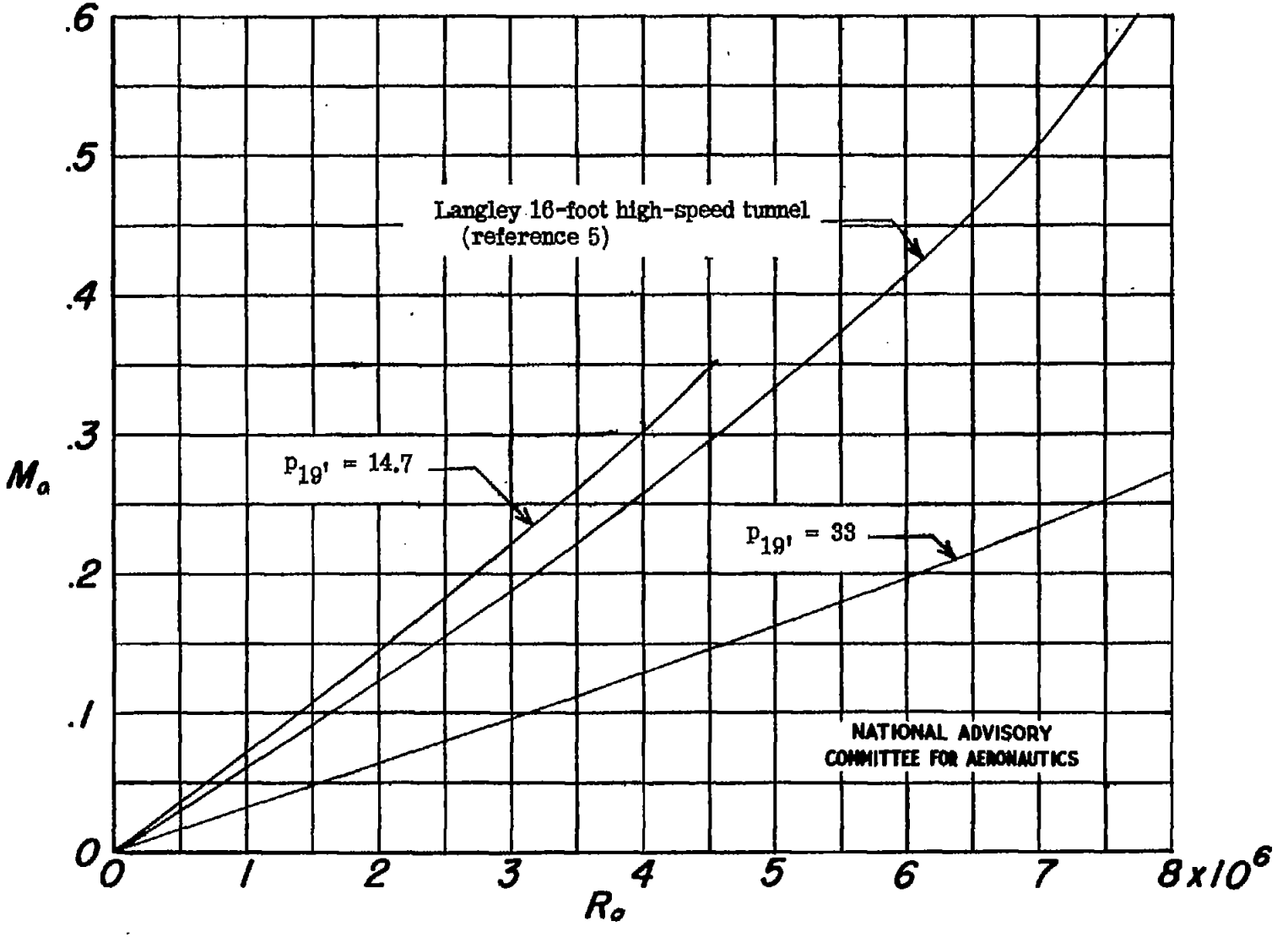

Figure 4.- Comparison of test conditions in the Langley 19-foot pressure tunnel and Langley 16-foot high-speed tunnel for a wing of NACA 230-series airfoil sections.

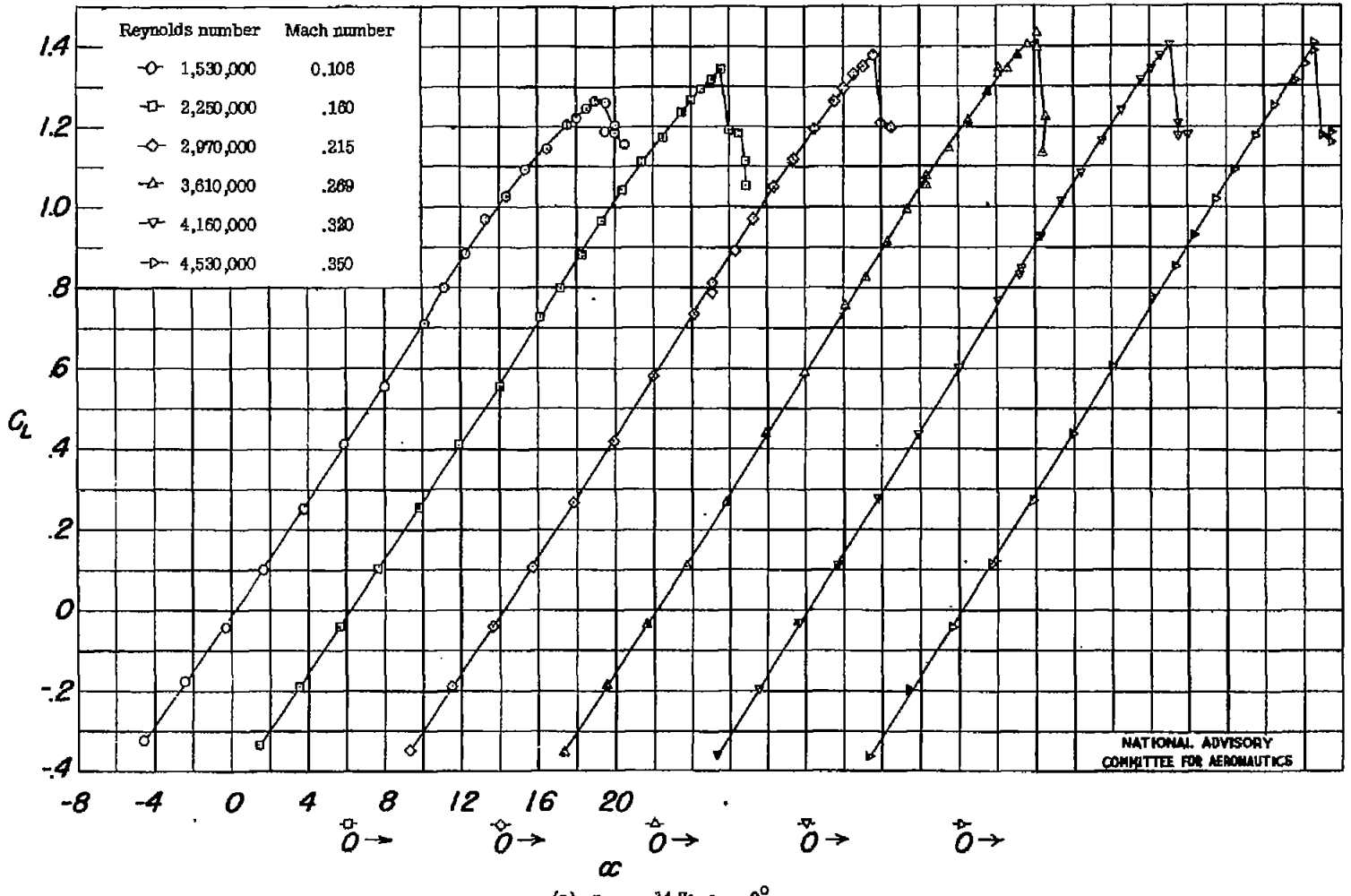

(a) $p_{19'} = 14.7$; $\delta_f = 0°$.

Figure 5.- Variation of lift coefficient with angle of attack for a wing of NACA 230-series airfoil sections tested in the Langley 19-foot pressure tunnel.

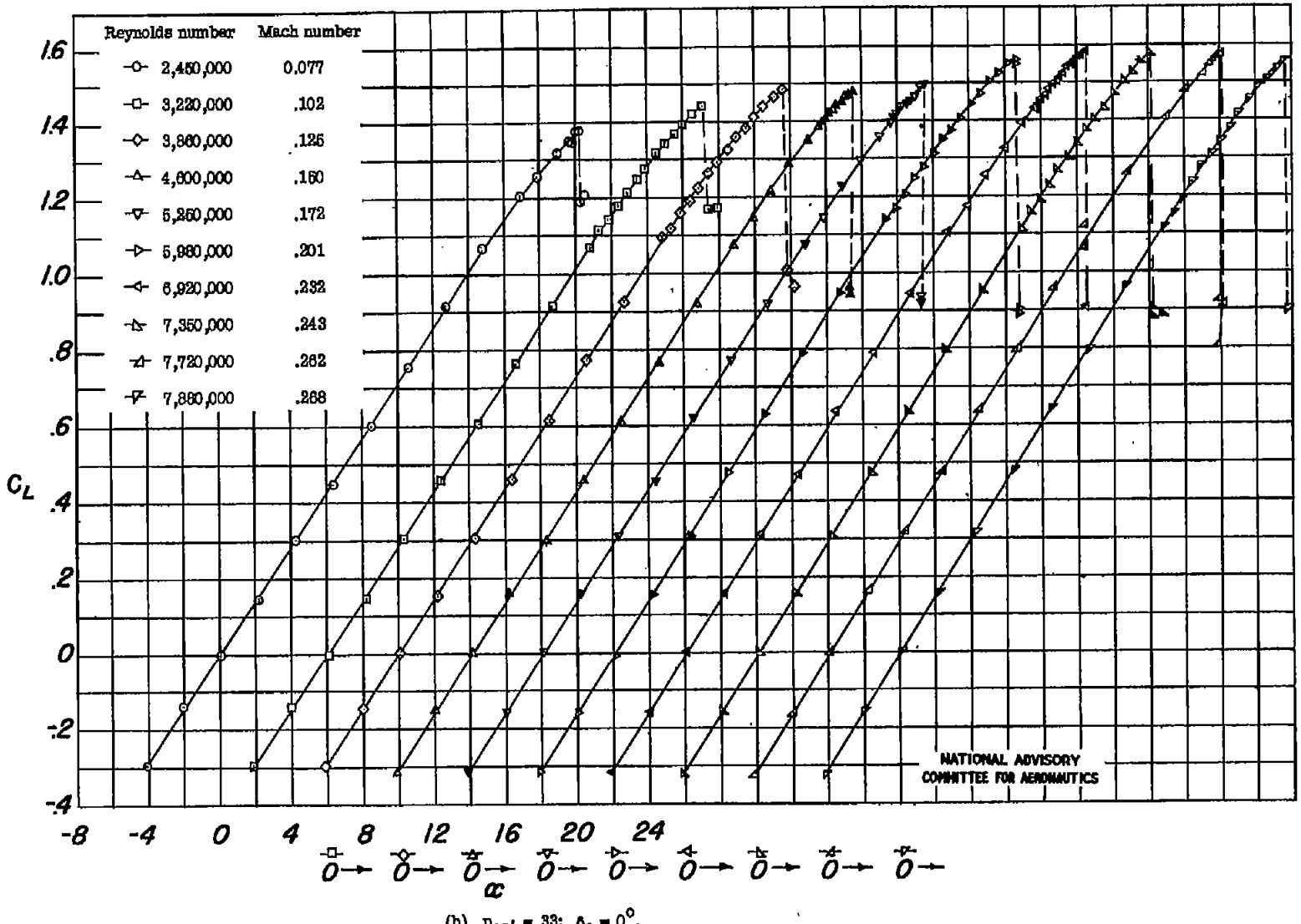

(b) $P_{1g'} = 33$; $\delta_f = 0^\circ$.

Figure 5.- Continued.

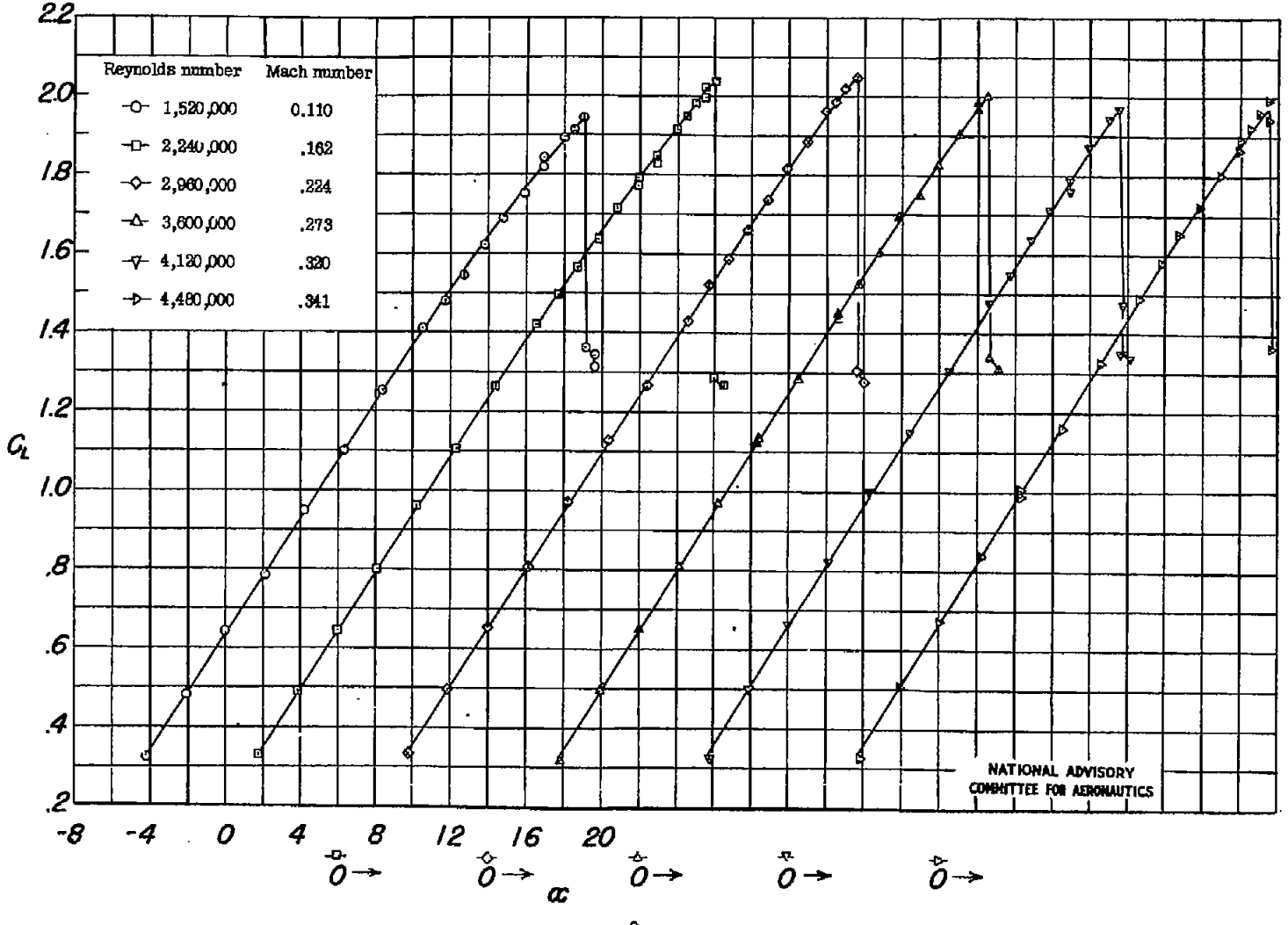

(c) $p_{19}' = 14.7$; $\delta_f = 60^\circ$ (partial span).

Figure 5.- Continued.

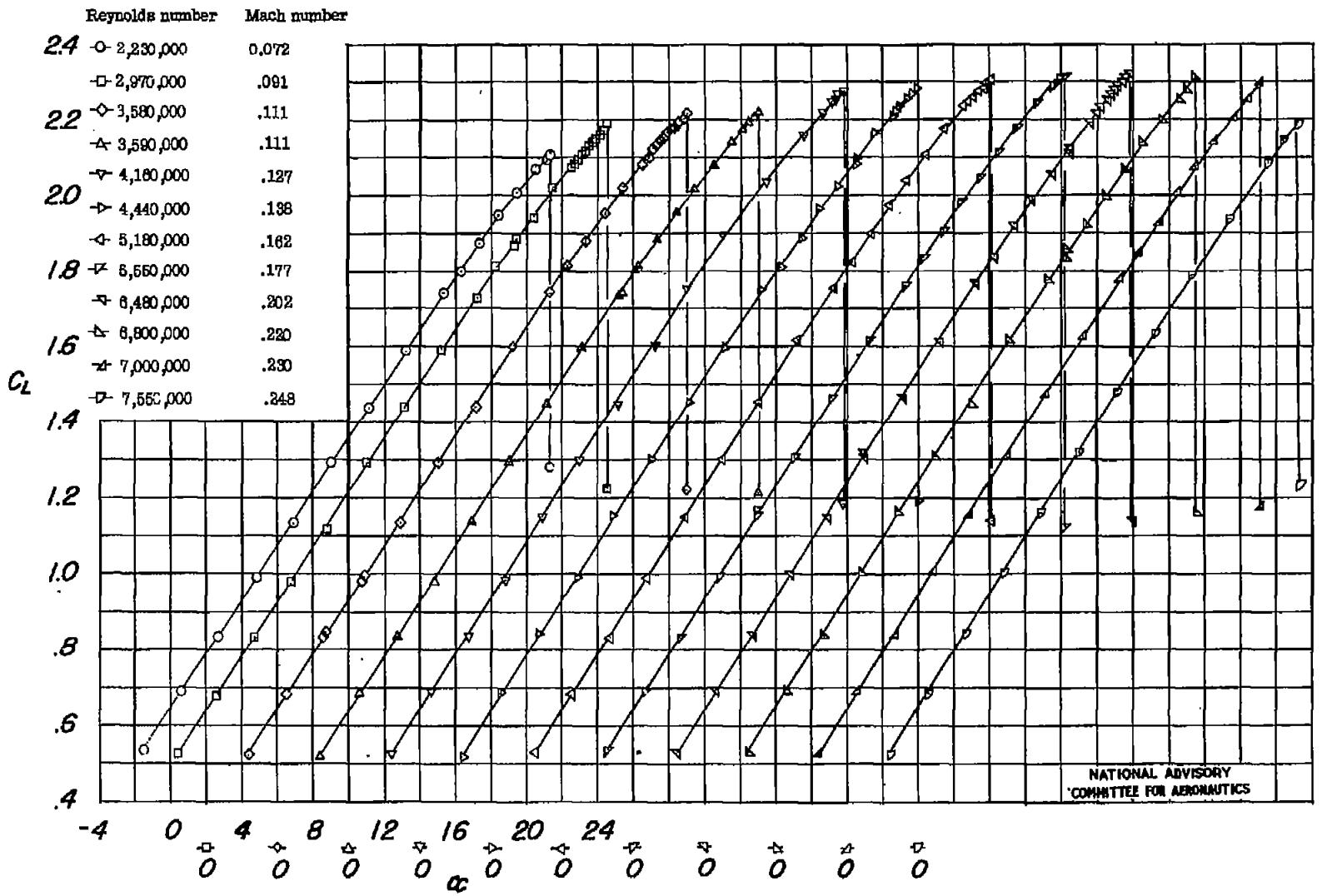

(d) $p_{19'} = 33$; $\delta_f = 60^\circ$ (partial span).

Figure 5.- Continued.

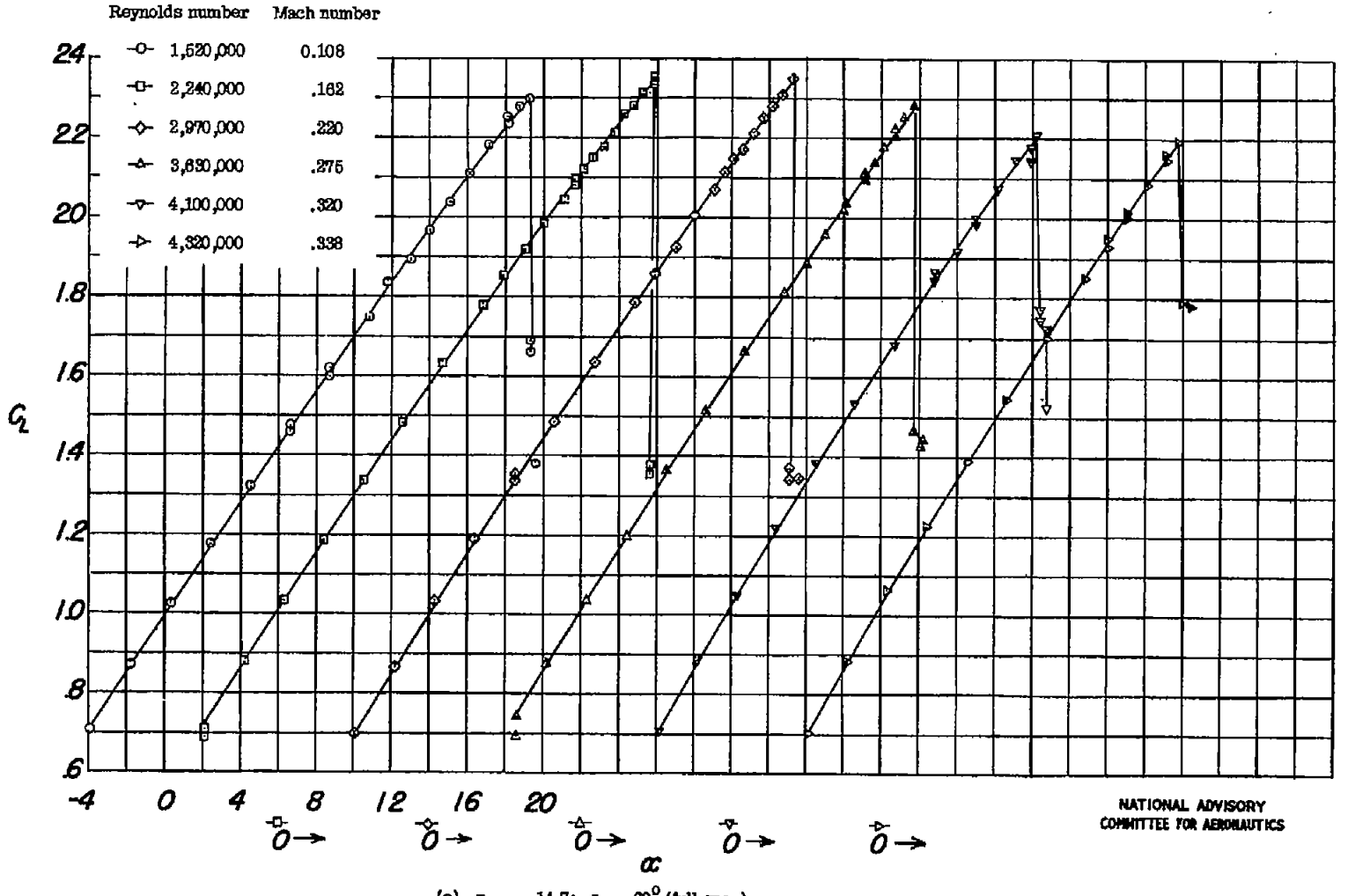

(e) $p_{19'} = 14.7$; $\delta_f = 60^\circ$ (full span).

Figure 5.- Continued.

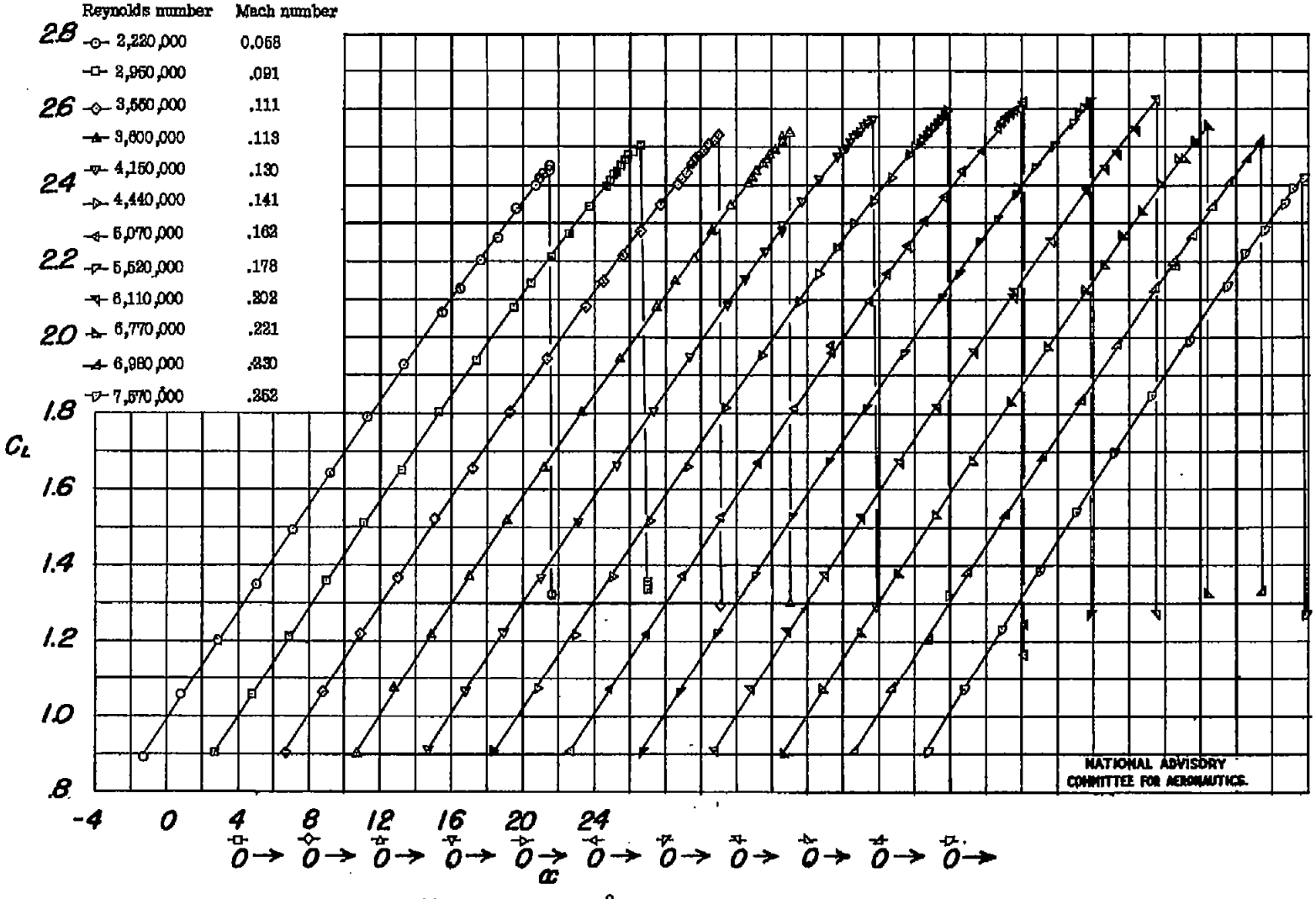

(f) $p_{1g'} = 33$; $\delta_f = 60^\circ$ (full span).

Figure 5.- Continued.

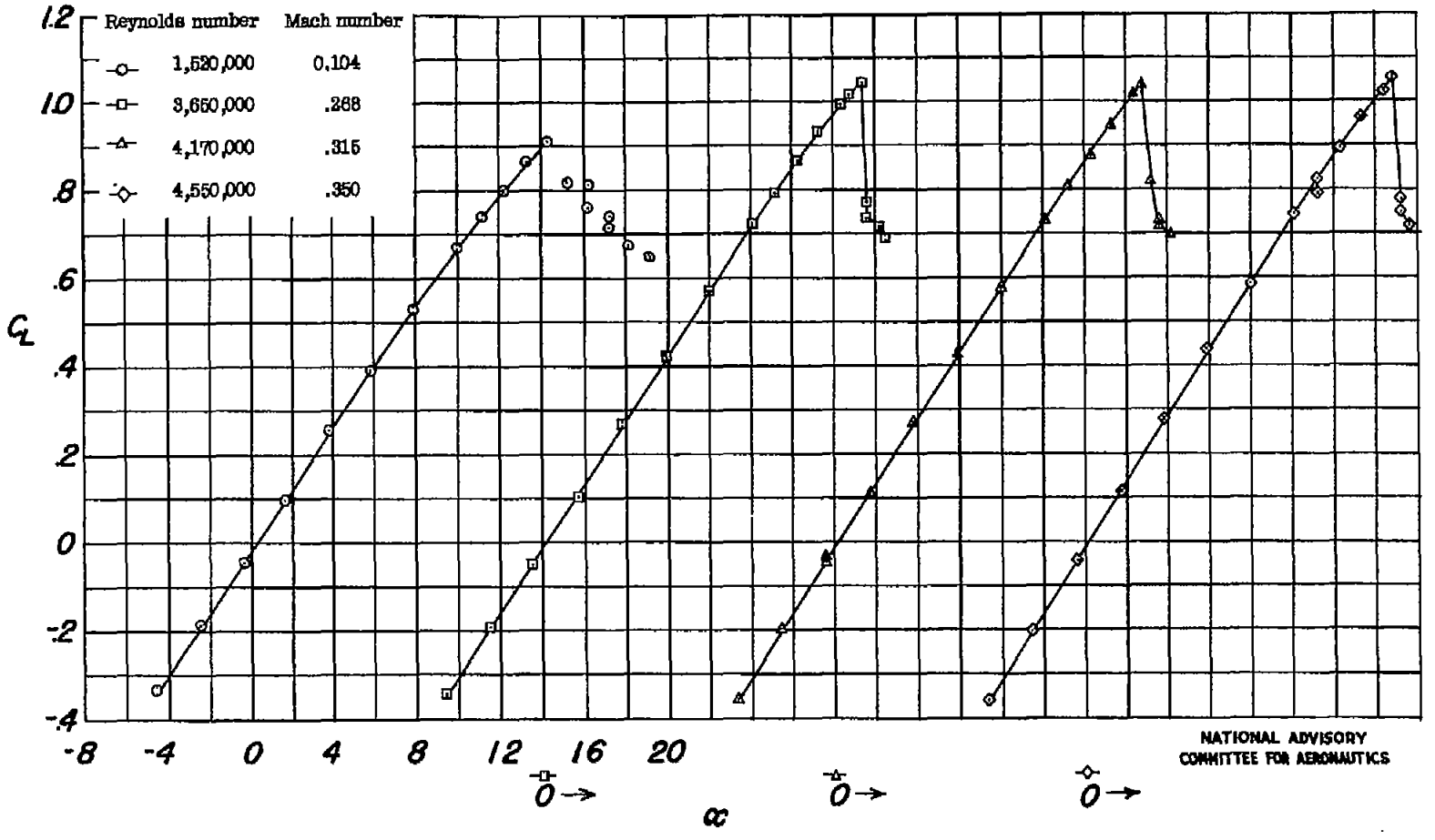

(g) $p_{19'} = 14.7$; $\delta_f = 0°$; leading-edge roughness .

Figure 5.- Continued .

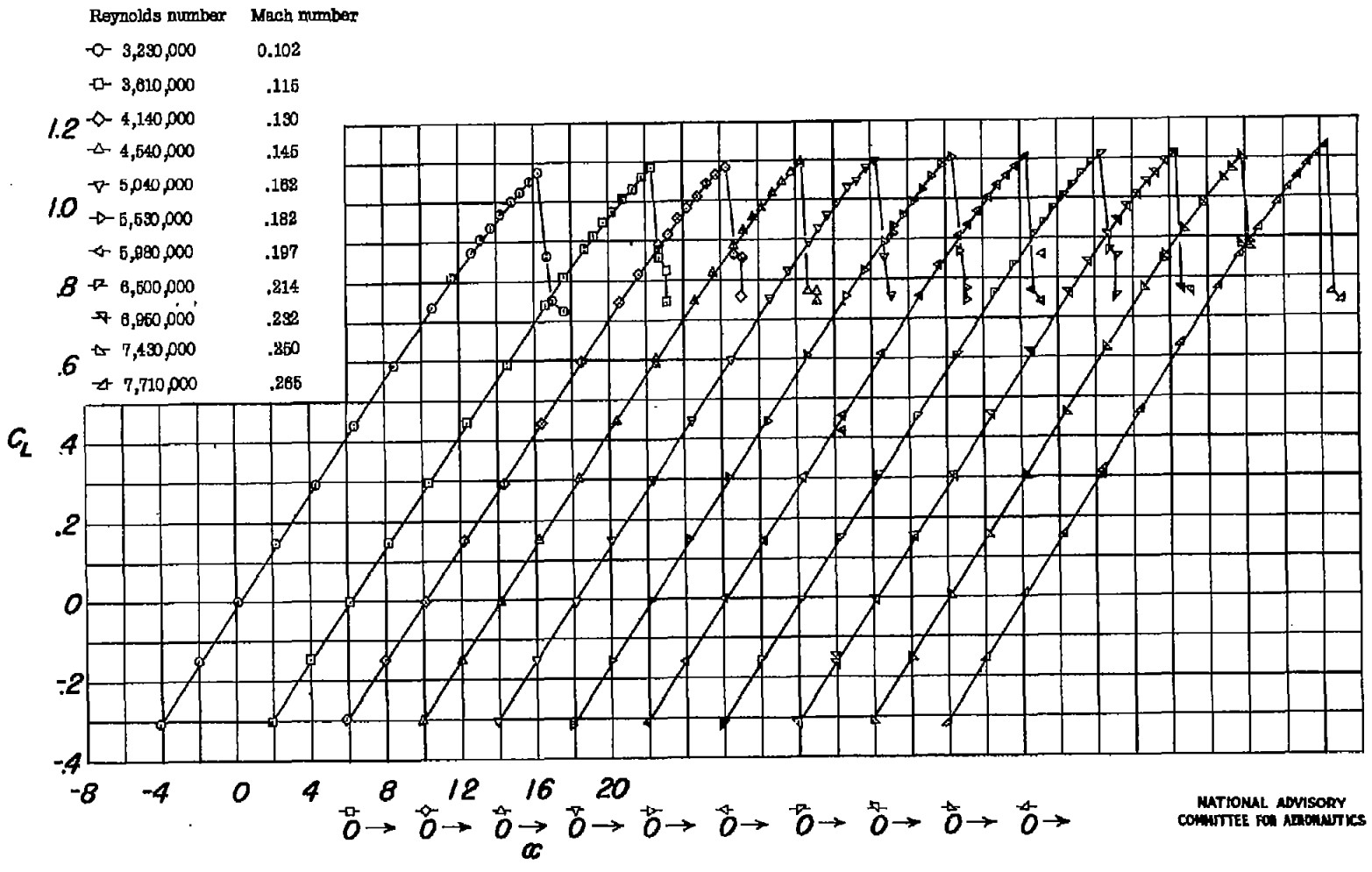

(h) $p_{19'} = 33$; $\delta_f = 0^\circ$; leading-edge roughness .

Figure 5.- Concluded.

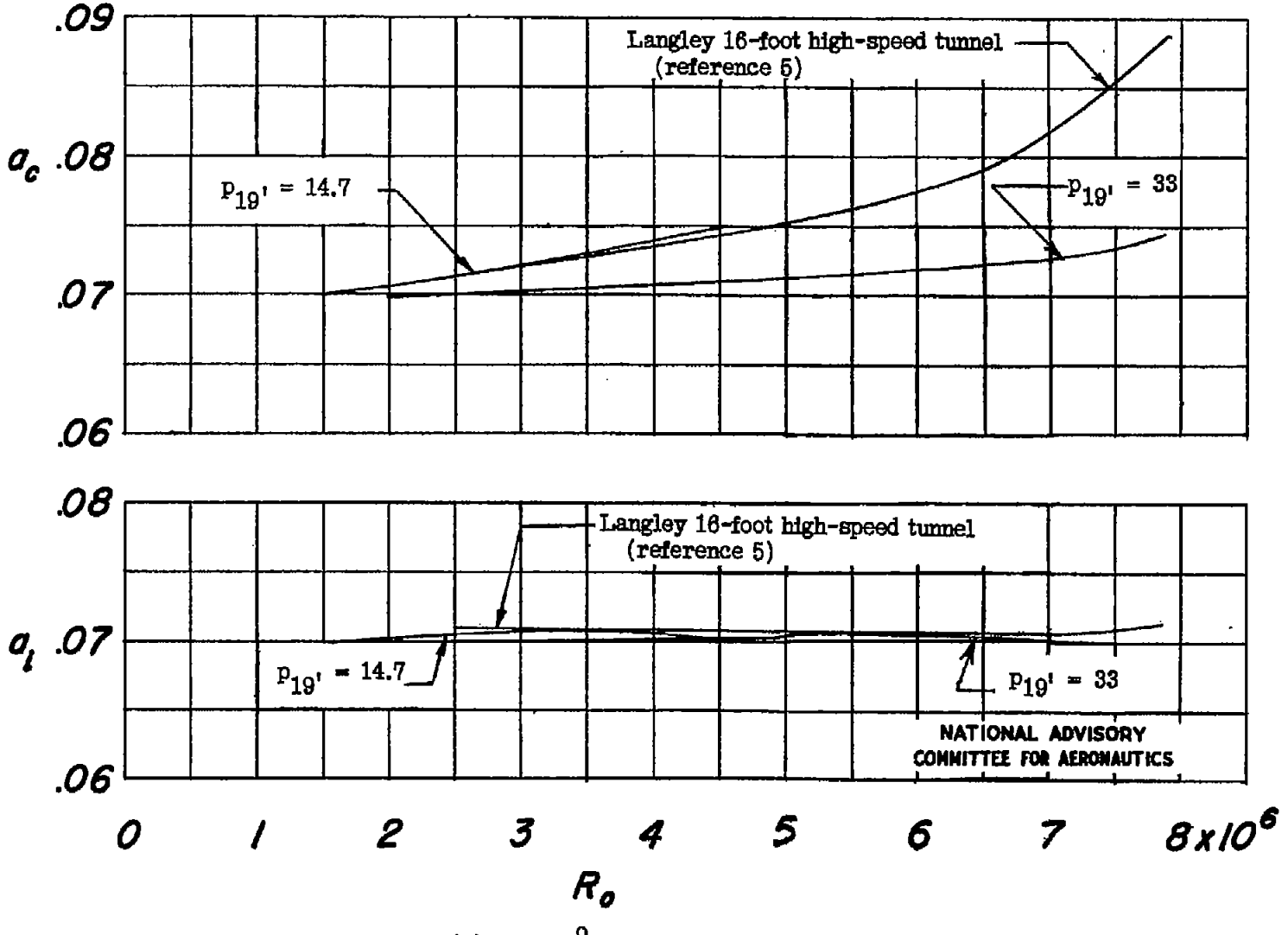

(a) $\delta_f = 0^\circ$.

Figure 6.- Variation of lift curve slopes with Reynolds number for the wing of NACA 230-series airfoil sections tested in the Langley 19-foot pressure tunnel.

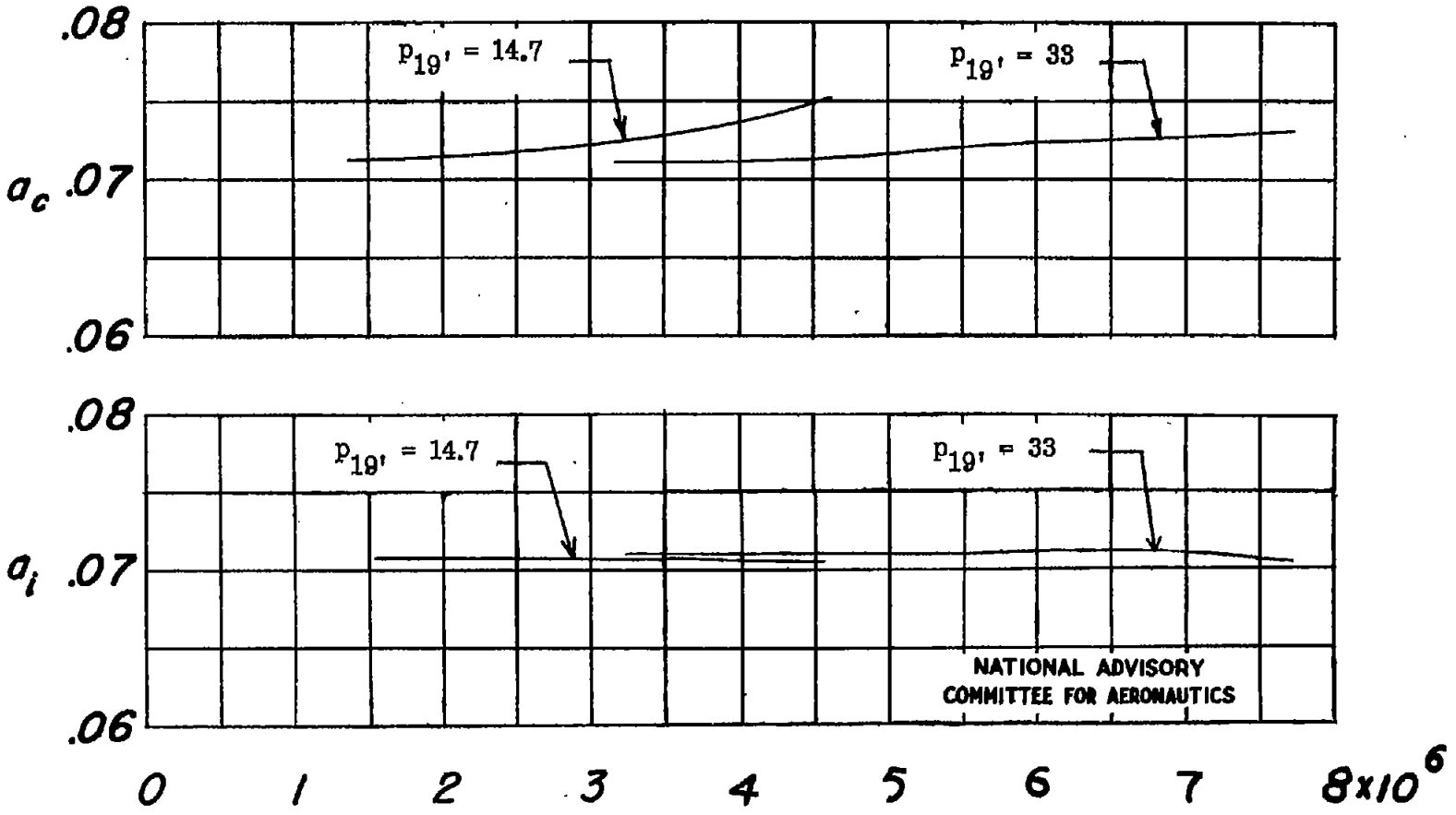

(b) $\delta_f = 0^\circ$; leading-edge roughness.

Figure 6.- Concluded.

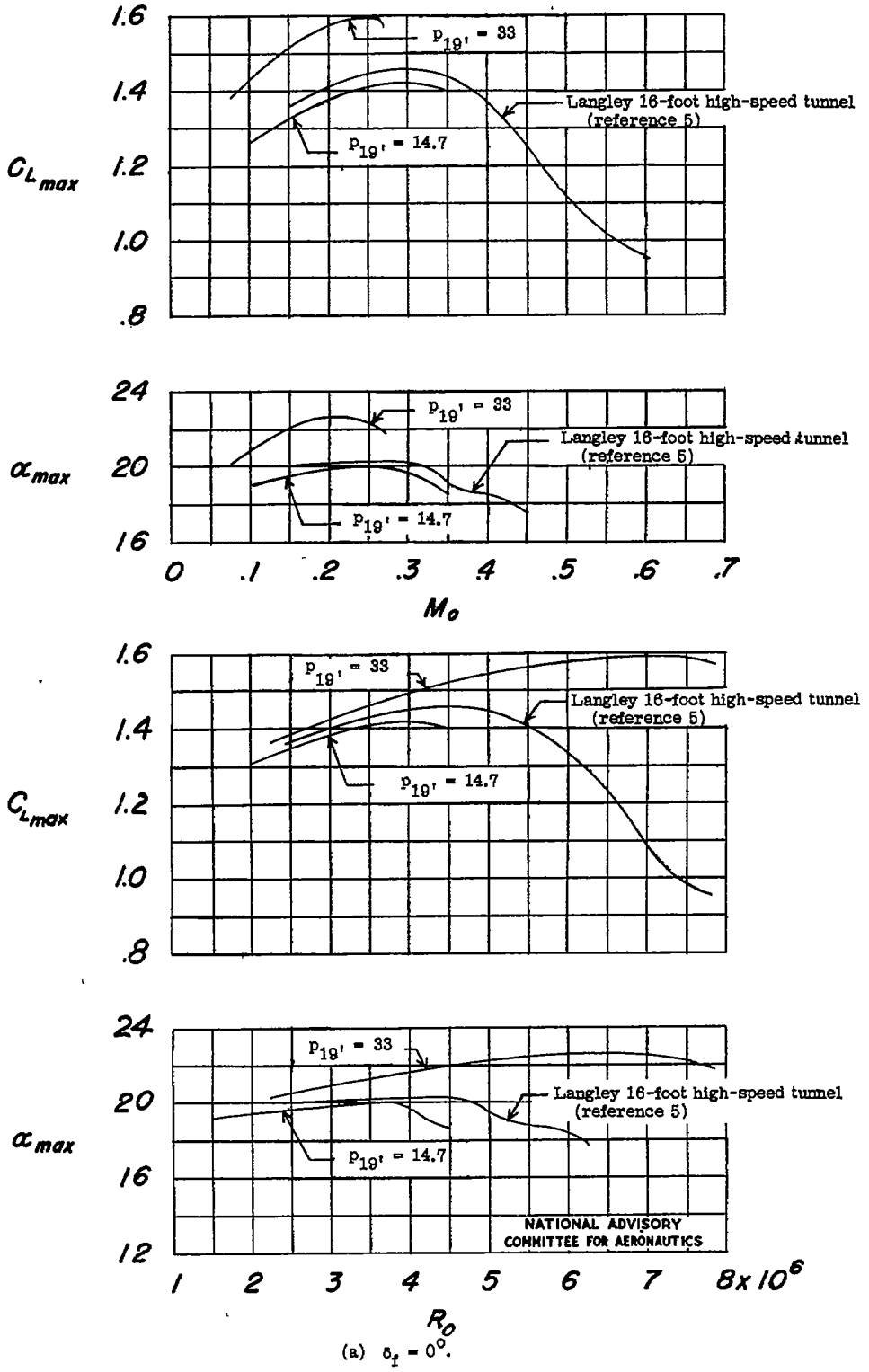

(a) $\delta_f = 0^\circ$.

Figure 7.- Variations of maximum lift coefficients and maximum angles of attack with Mach number and Reynolds number for wing of NACA 230-series airfoil sections tested in the Langley 19-foot pressure tunnel.

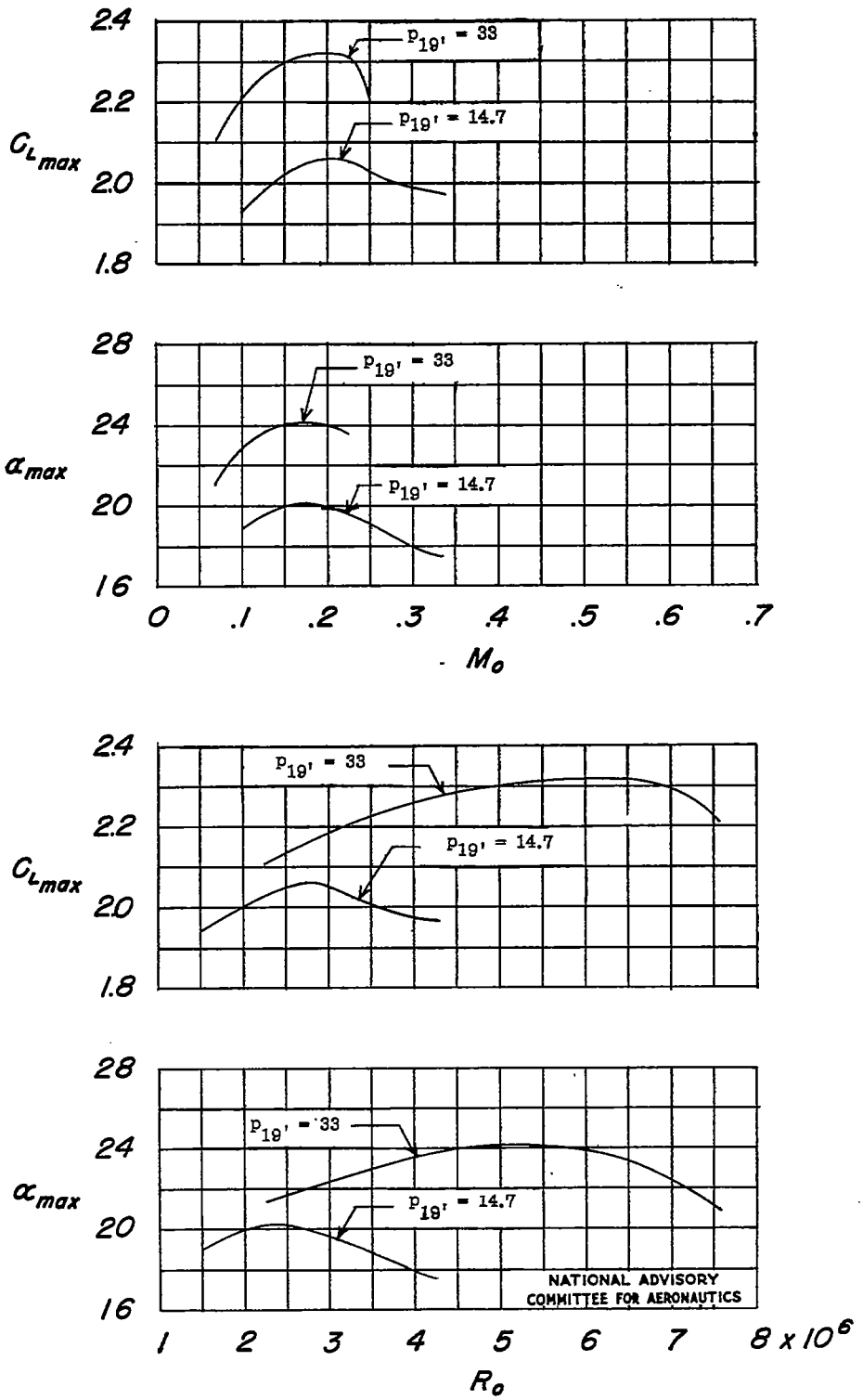

(b) $\delta_f = 60^\circ$ (partial span).

Figure 7.- Continued.

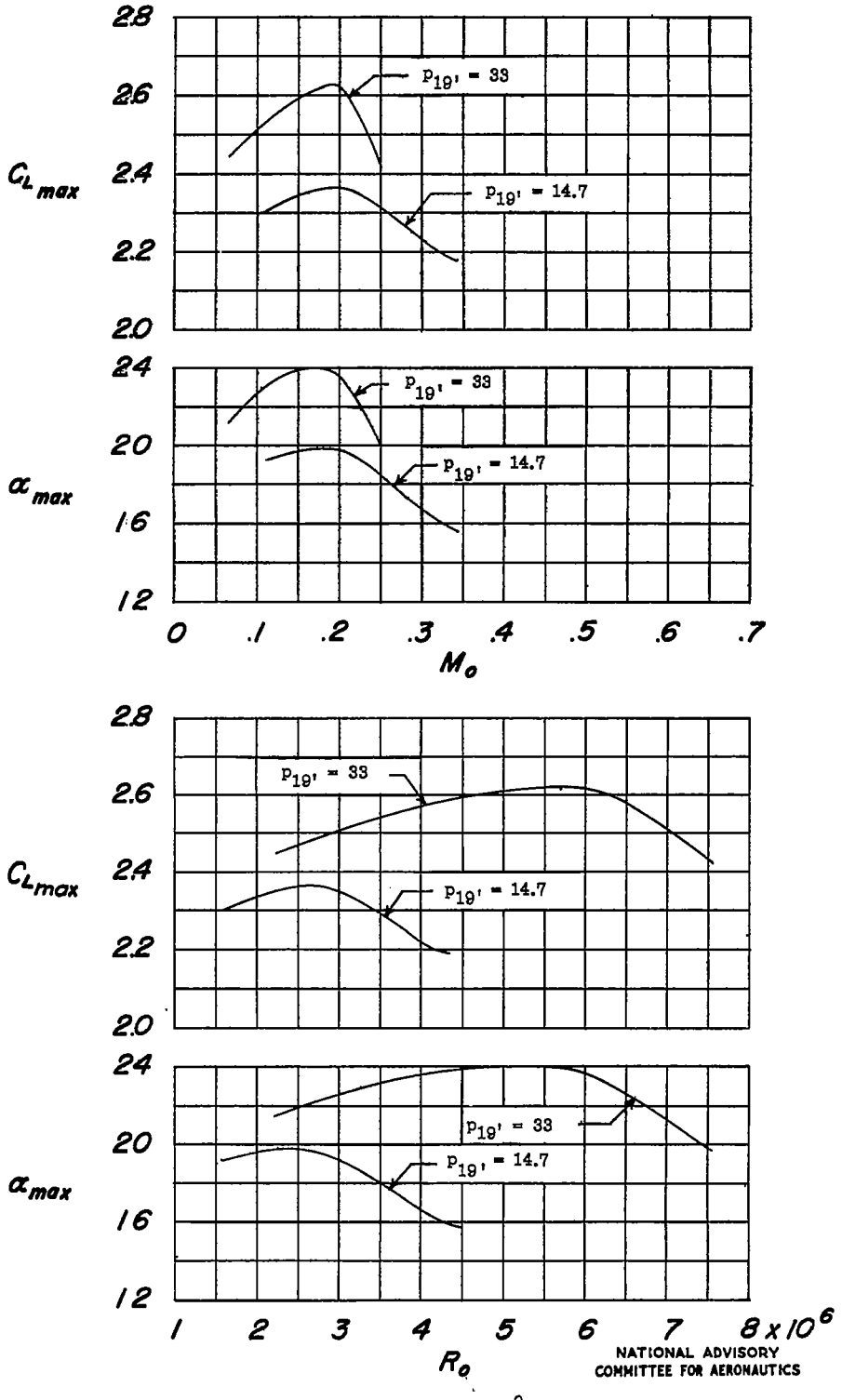

(c) $\delta_f = 60^\circ$ (full span).

Figure 7.- Continued.

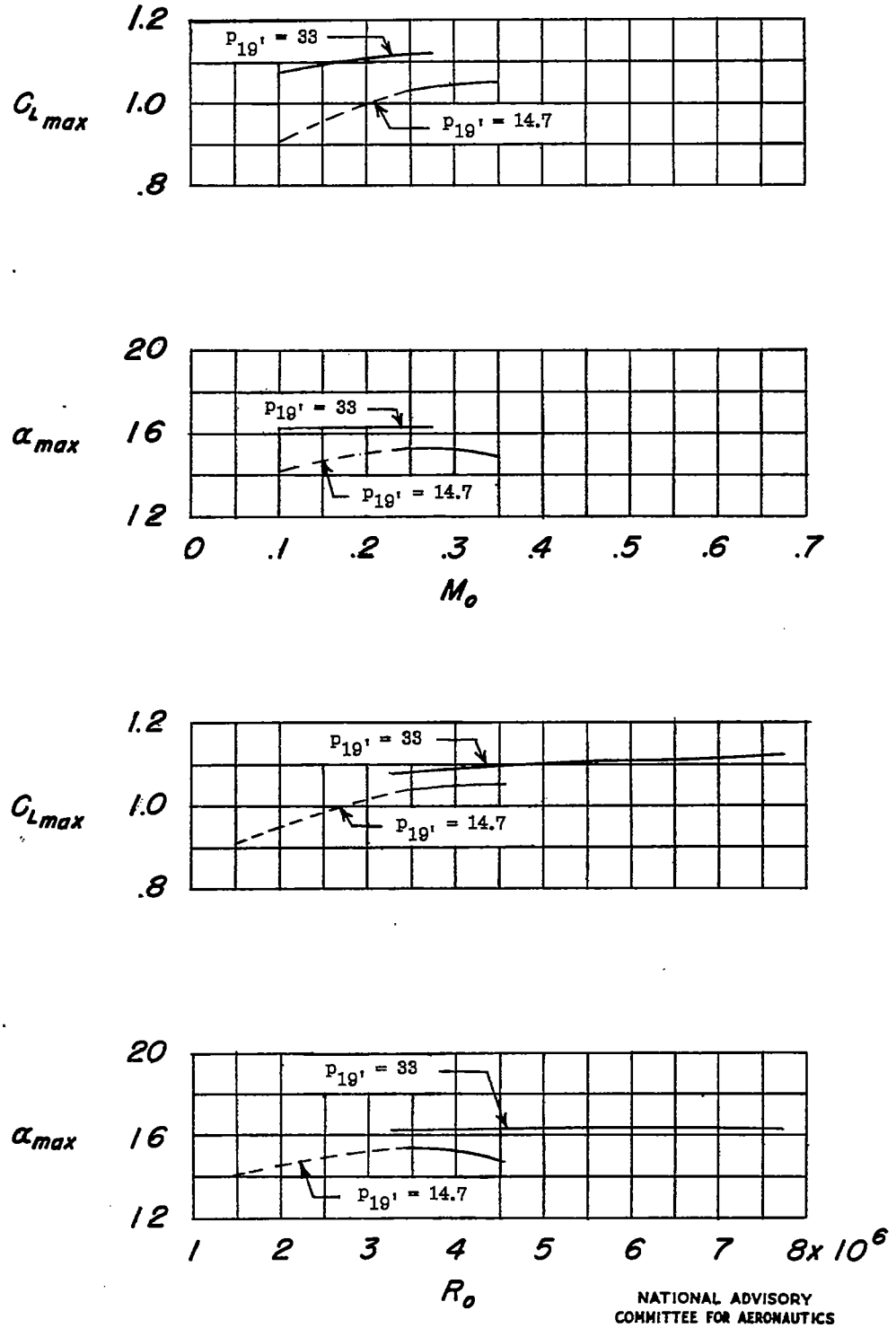

(d) $\delta_f = 0^\circ$; leading-edge roughness.

Figure 7.- Concluded.

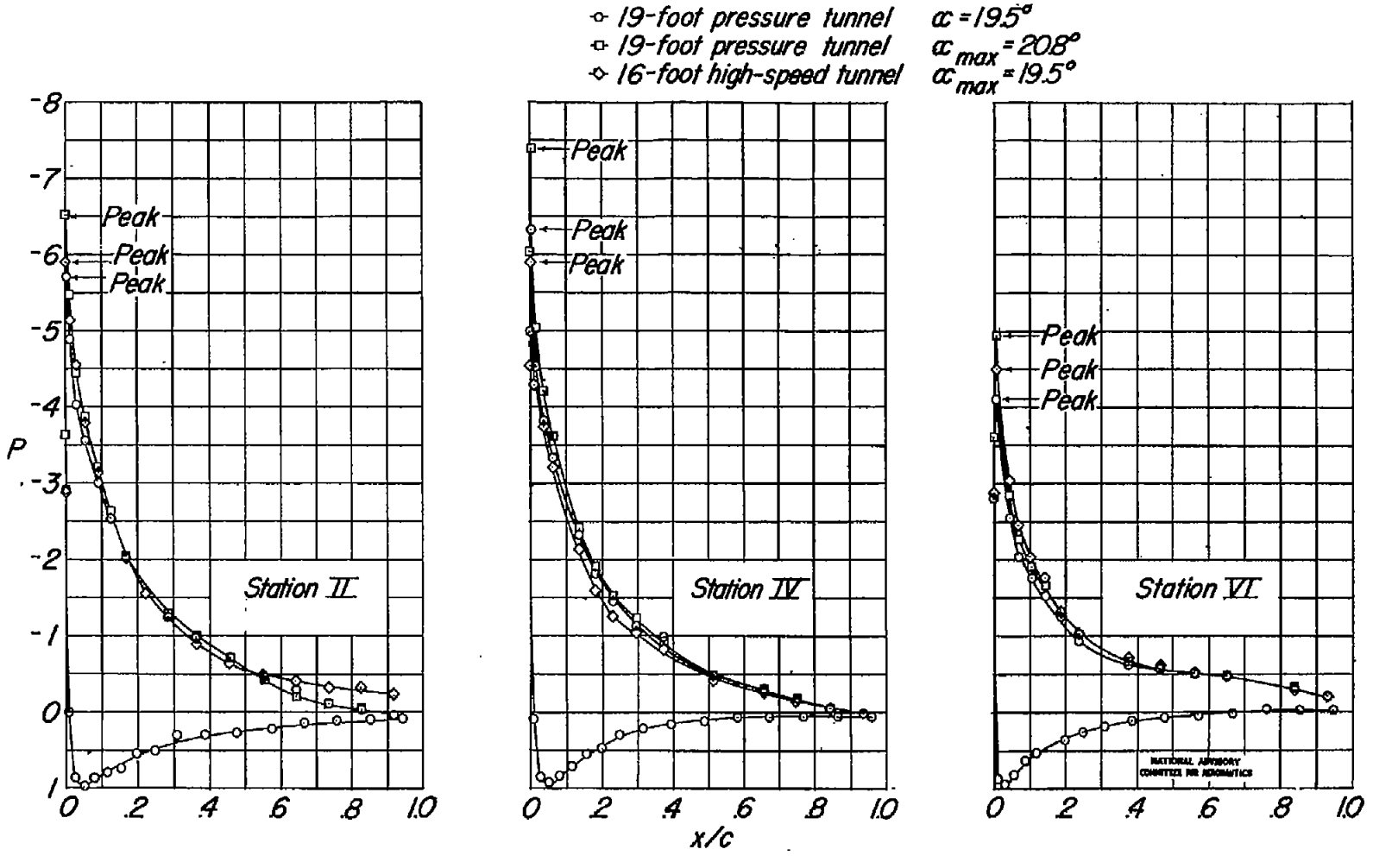

Figure 8.- Comparison of chordwise pressure distribution over a wing of NACA 230-series airfoil sections tested in the Langley 19-foot pressure tunnel at $M_o = 0.10$, $R_o = 3{,}220{,}000$ and in the Langley 16-foot high-speed tunnel at $M_o = 0.10$, $R_o = 1{,}650{,}000$, $\delta_f = 0^\circ$.

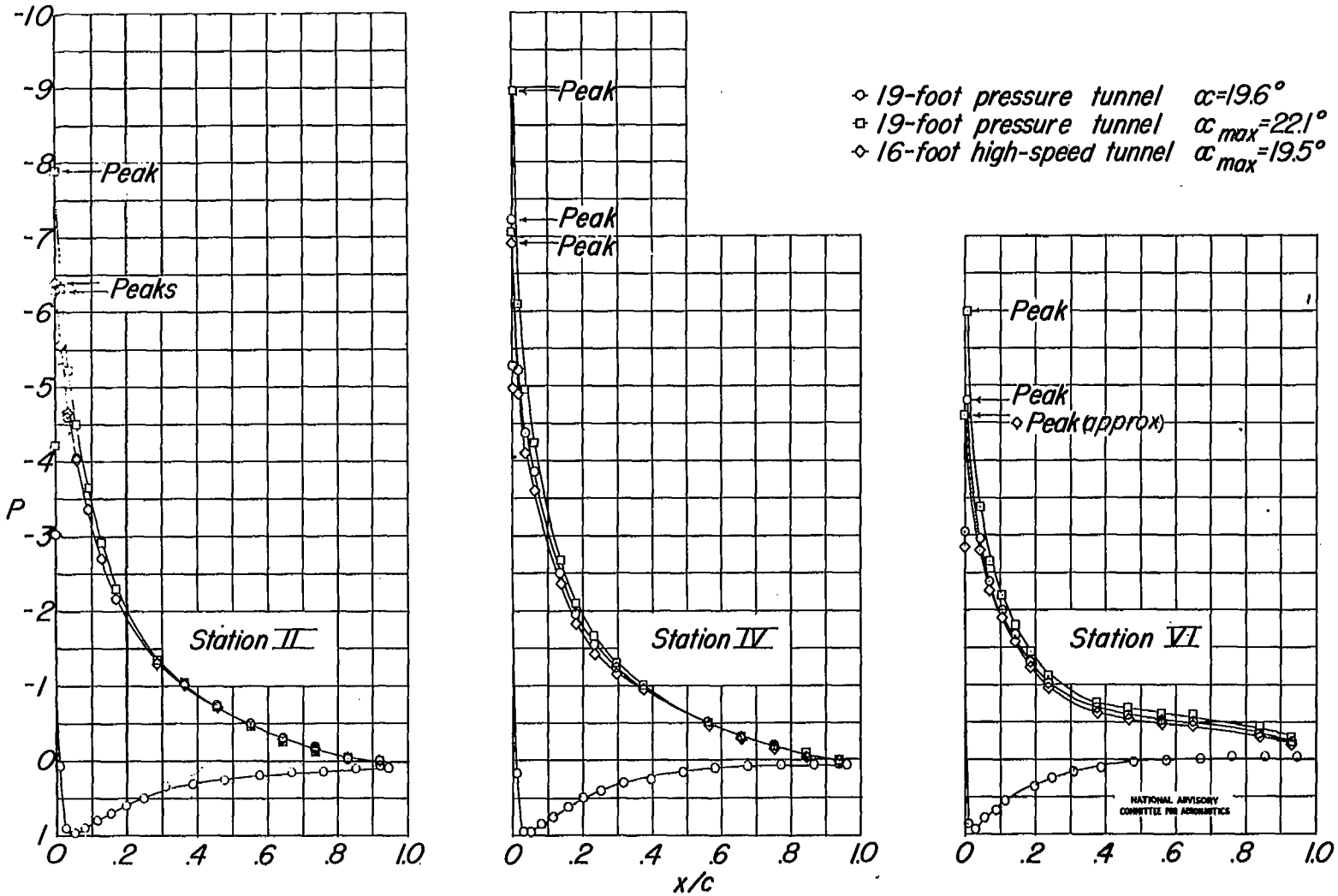

Figure 9.- Comparison of chordwise pressure distribution over a wing of NACA 230-series airfoil sections tested in the Langley 19-foot pressure tunnel at $M_o = 0.25$, $R_o = 7{,}490{,}000$ and in the Langley 16-foot high-speed tunnel at $M_o = 0.25$, $R_o = 3{,}920{,}000$. $\delta_f = 0^\circ$.

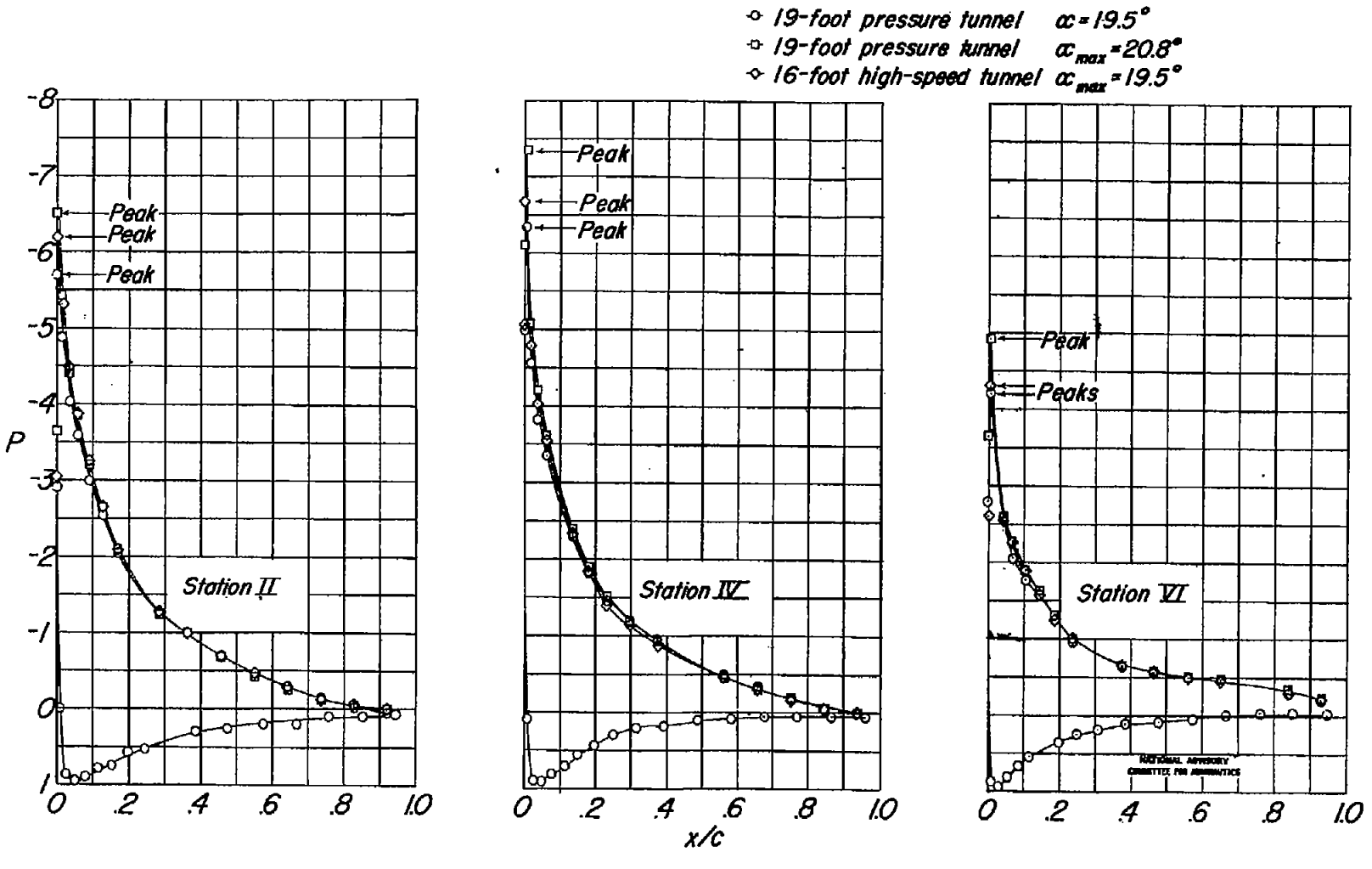

Figure 10.- Comparison of chordwise pressure distribution over a wing of NACA 230-series airfoil sections tested in the Langley 19-foot pressure tunnel at $M_o = 0.10$, $R_o = 3{,}220{,}000$ and in the Langley 16-foot high-speed tunnel at $M_o = 0.20$, $R_o = 3{,}170{,}000$. $\delta_f = 0°$.

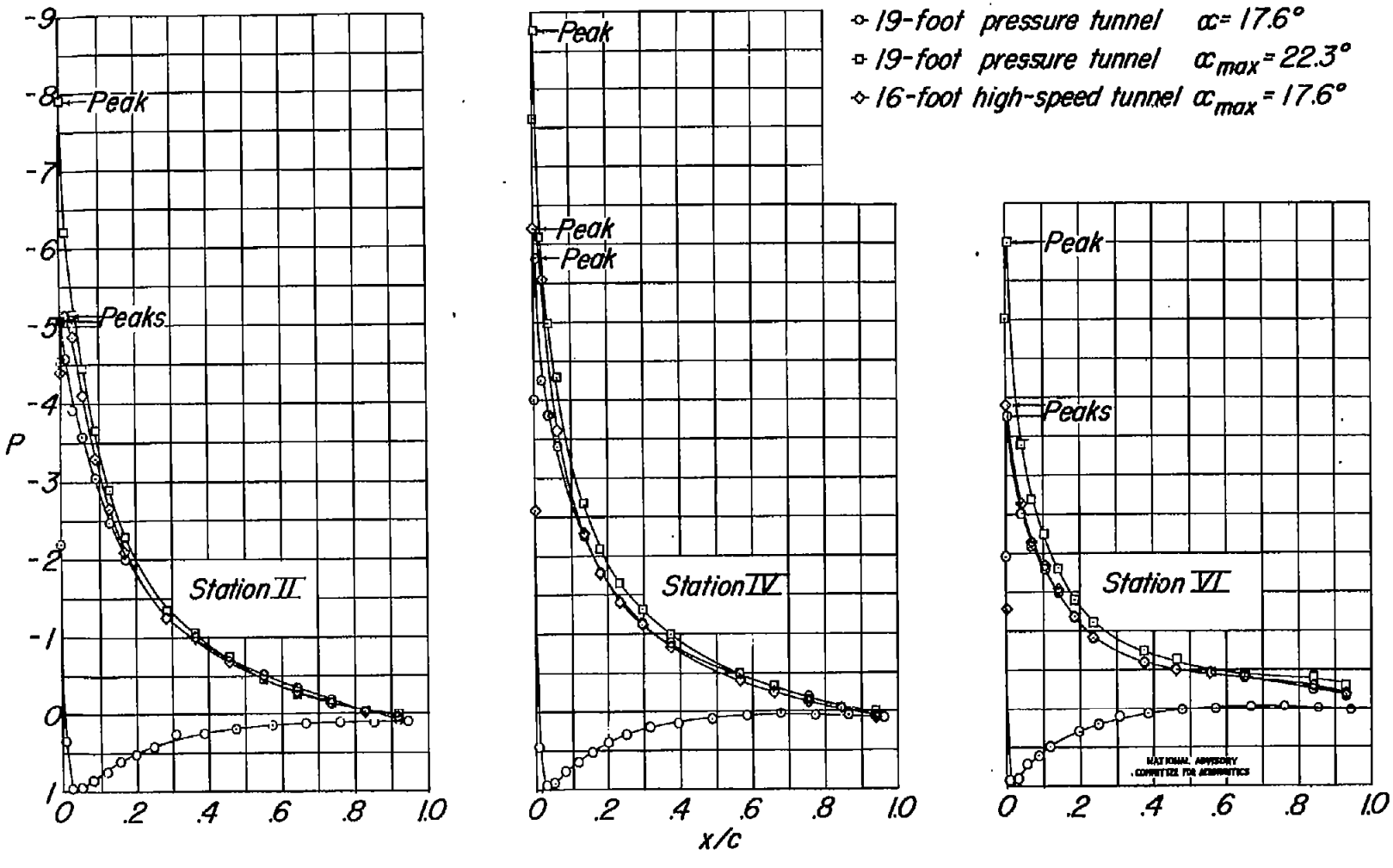

Figure 11.- Comparison of chordwise pressure distribution over a wing of NACA 230-series airfoil sections tested in the Langley 19-foot pressure tunnel at $M_0 = 0.20$, $R_0 = 5,900,000$ and in the Langley 16-foot high-speed tunnel at $M_0 = 0.40$, $R_0 = 5,850,000$. $\delta_f = 0^\circ$.

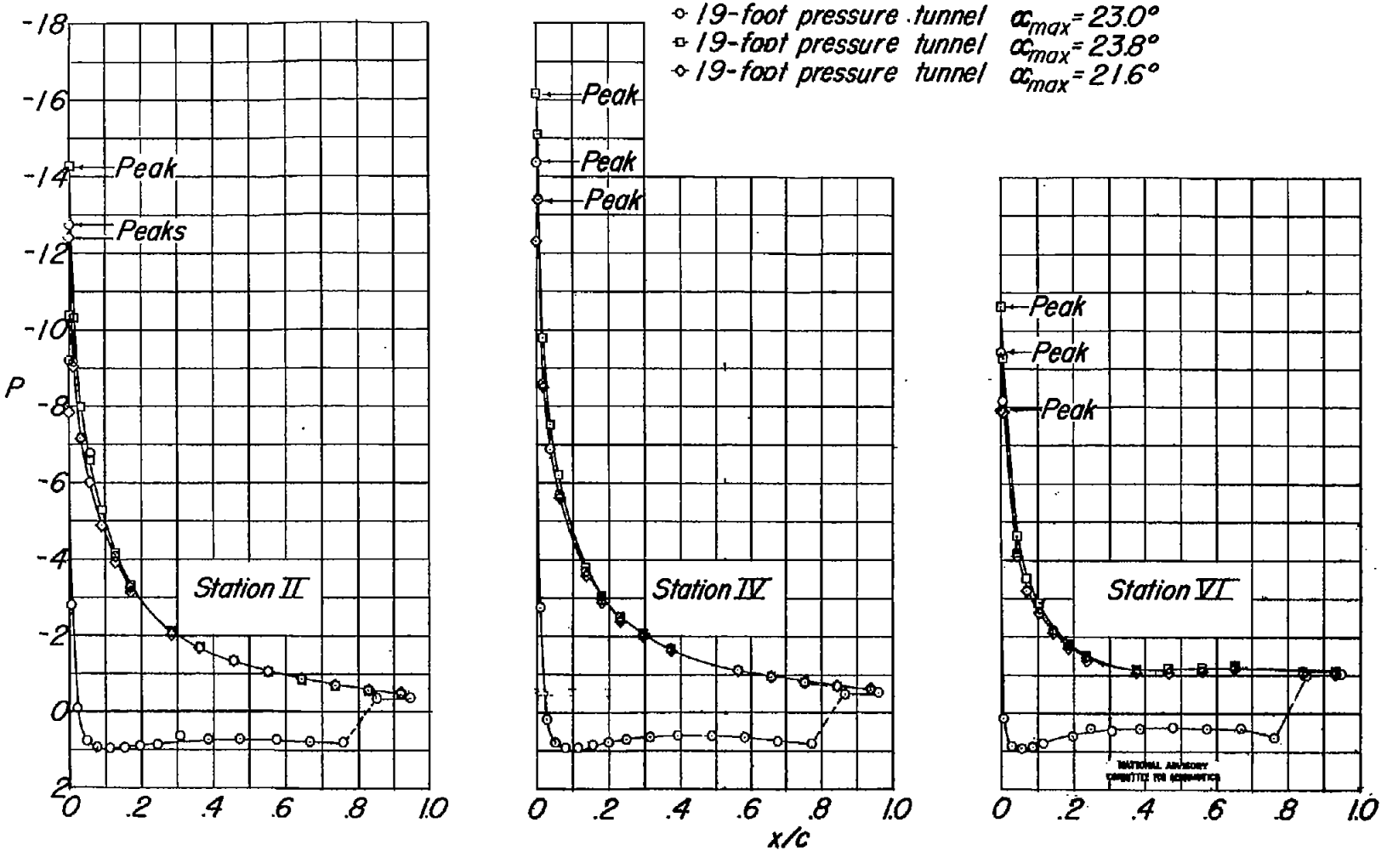

Figure 12.- Comparison of chordwise pressure distribution over a wing of NACA 230-series airfoil sections tested in the Langley 19-foot pressure tunnel at $M_o = 0.11$ and $R_o = 3,510,000$ for $\alpha_{max} = 23.0°$, $M_o = 0.16$ and $R_o = 5,020,000$ for $\alpha_{max} = 23.8°$, and $M_o = 0.22$ and $R_o = 6,770,000$ for $\alpha_{max} = 21.6°$. $\delta_f = 60°$ (full span).

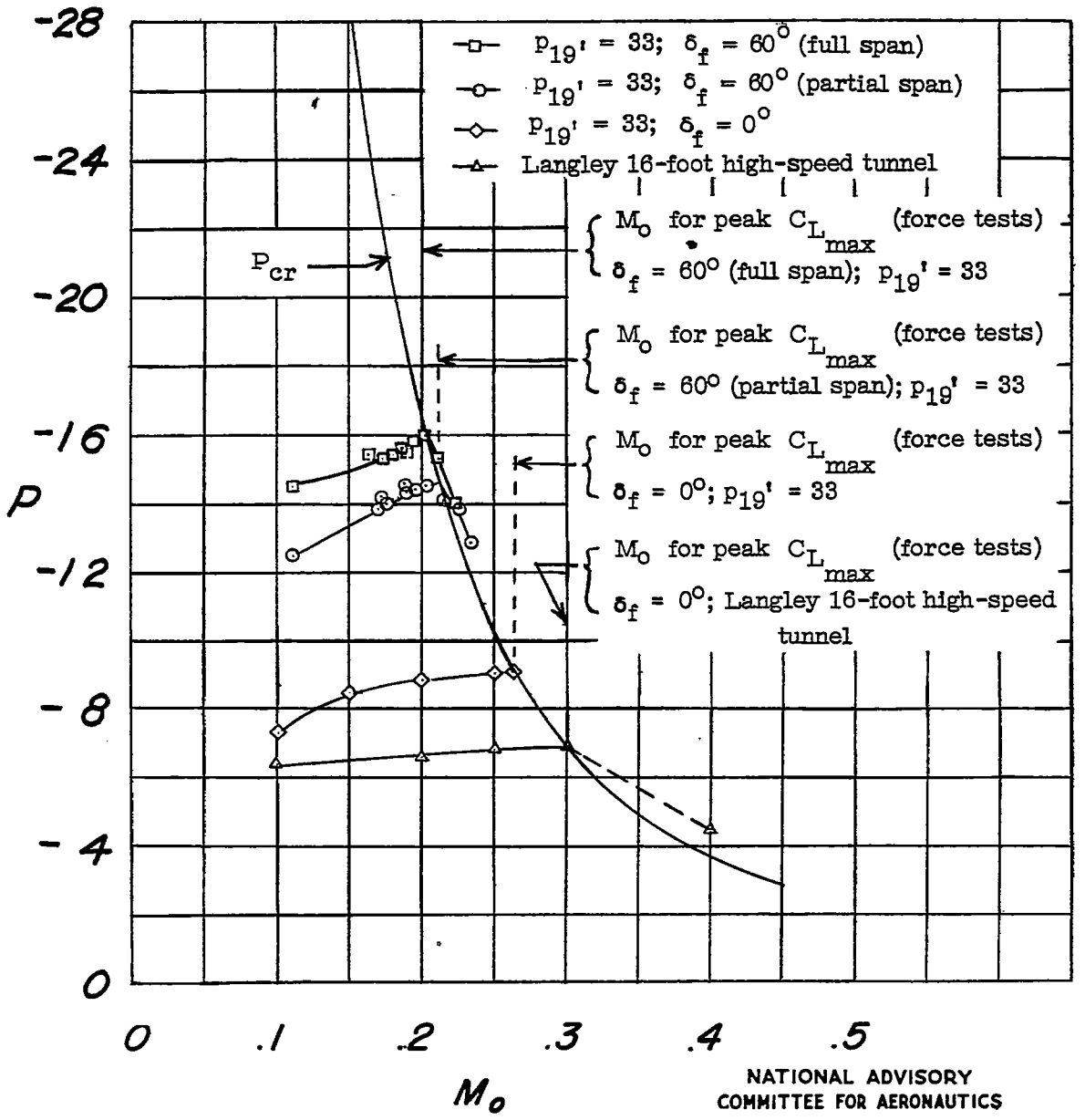

Figure 13.- Variations of maximum wing pressure coefficients with Mach number for a wing of NACA 230-series airfoil sections tested in the Langley 19-foot pressure tunnel.

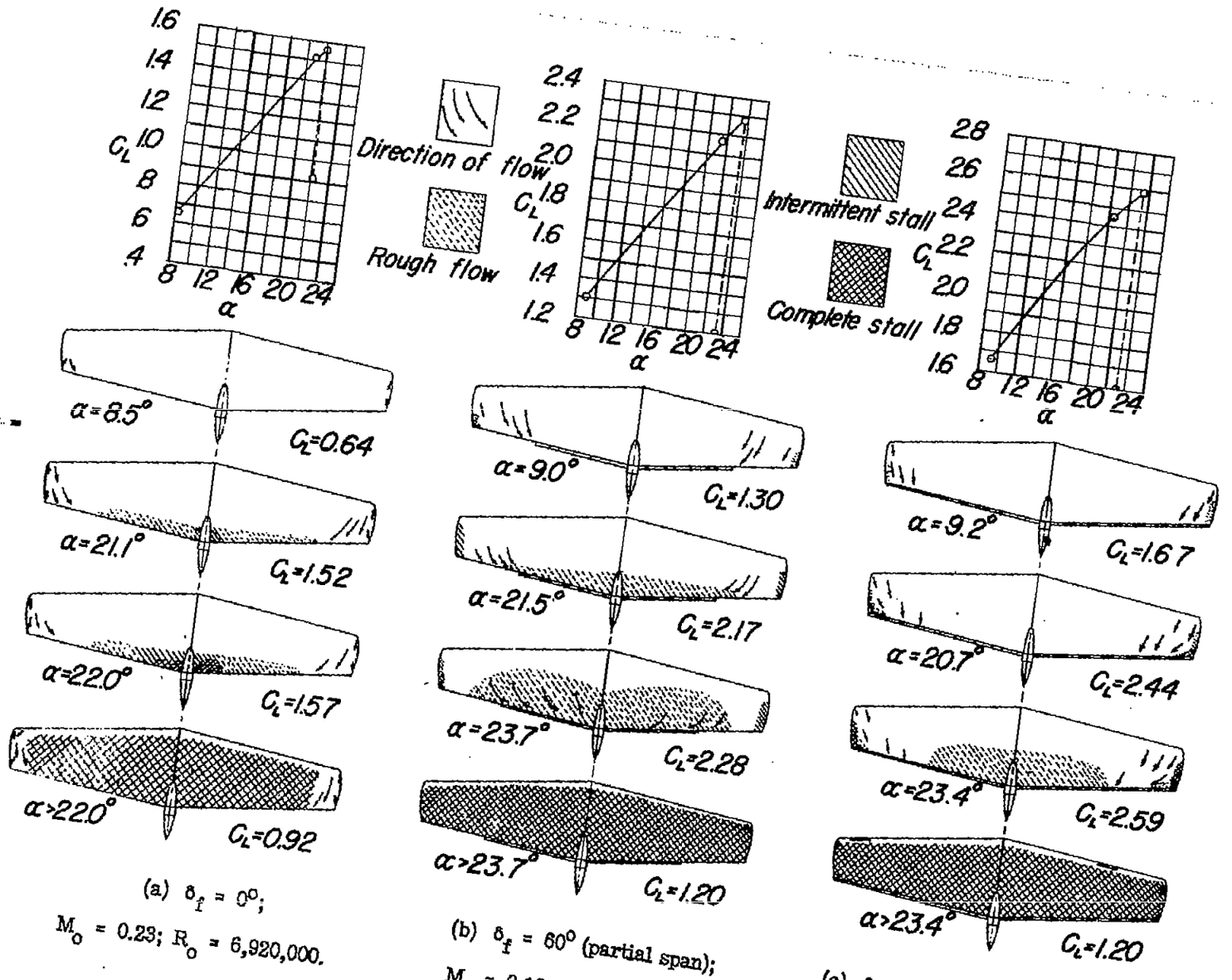

(a) $\delta_f = 0^\circ$; $M_o = 0.23$; $R_o = 6{,}920{,}000$.

(b) $\delta_f = 60^\circ$ (partial span); $M_o = 0.16$; $R_o = 5{,}180{,}000$.

(c) $\delta_f = 60^\circ$ (full span); $M_o = 0.16$; $R_o = 5{,}180{,}000$.

Figure 14.- Stall pattern of wing of NACA 230-series airfoil sections.